12-2017

3D Printed PCU/UHMWPE Polymeric Blends for Artificial Knee Meniscus

Raissa Araujo Borges
University of Arkansas, Fayetteville

3D Printed PCU/UHMWPE Polymeric Blends for Artificial Knee Meniscus

A thesis submitted in partial fulfillment
of the requirements for the degree of
Master of Science in Mechanical Engineering

by

Raissa Araujo Borges
Universidade Federal de Pernambuco
Bachelor of Science in Mechanical Engineering, 2015

December 2017
University of Arkansas

This thesis is approved for recommendation to the Graduate Council.

_____
Min Zou, Ph.D.
Thesis Director

_____
Jingyi Chen, Ph.D.
Committee Member

_____
Steve Tung, Ph.D.
Committee Member

ABSTRACT

3D printing was used to fabricate porous artificial knee meniscus material from biocompatible polymeric blends of polycarbonate-urethane (PCU) and ultra-high-molecular-weight polyethylene (UHMWPE) to enable "weep" lubrication that mimics the native meniscus. 3D printed and molded pure PCU, as well as molded PCU and UHMWPE, were used for comparison. Preliminary printing was done to evaluate the impact of process parameters on the results. The samples were subject to a variety of rotational oscillating friction and wear tests under simulated body fluid and loading conditions to replicate the natural motion of the knee. Results show that 3D printed PCU samples yielded a 27% wear depth reduction compared to molded PCU samples, which may be attributed to their porous structure and flexibility. The cross-sectional area of the 3D printed blend and pure PCU samples showed 13.61% and 6.34% porosity, respectively, while no porosity was observed on the molded PCU and UHMWPE samples. The porosity of 3D printed PCU samples enabled them to absorb 46% more fluid than its molded version. These findings support 3D printing method as a good alternative to fabricate highly porous, customizable PCU implants that mimic the lubrication mechanisms of the native meniscus.

ACKNOWLEDGEMENTS

First, I would like to extend my gratitude to my advisor, Dr. Min Zou, who has provided me the opportunity to pursue my masters at the University of Arkansas as part of her research group. Her guidance, support and encouragement throughout my course at the University of Arkansas have enabled me to achieve new heights in my career. Her kindness, patience, boldness and enthusiasm have truly inspired me along the way, motivating me to strive for excellent in each step. I have learned considerably from her, not only about technical and academic matters, but also through her great leadership values.

I would like to thank Dr. Steve Tung and Dr. Jingyi Chen for serving on my thesis committee. I also thank Dr. Dipankar Choudhury for the valuable discussions, academic and life lessons, and all the advice on my research. His knowledge and excitement about biotribology have guided me through my project. I would like to thank my colleagues at the Nano Mechanics and Tribology Lab for the dialogues, insights and help in the lab. In particular, I would like to thank Josh Goss for his tremendous and prompt assistance in the lab. I have enjoyed the company of all of them, which certainly contributed to the successfully completion of my experiments.

Many thanks to the University of Arkansas for the resources and for providing a welcoming environment for me since the beginning. I have been involved with incredible and supportive groups, who have provided me with joyful learning experiences. I thank the Arkansas Biosciences Institute and the University of Arkansas for major equipment funding support, as well as the Arkansas Nano & Bio Materials Characterization Facility and the High-Density Electronics Center for equipment use. Funding support for this work was provided by Arkansas Biosciences Institute and the US National Science Foundation (NSF) under Grant No. OIA-1457888 from the Center for Advanced Surface Engineering and the Arkansas EPSCoR Program, ASSET III.

Finally, but equally important, I want to show my great appreciation to the support and understanding of my new and old friends, as well as my family. They all have been present in both good and stressful phases, regardless the distance between us. I could not have made it here without the encouragement of my parents, who have given me emotional support and invested on my education in my entire life. A special thanks to my partner Leonardo for always caring and giving me strength, through advice or by simply listening to me. His support has given me confidence and helped me achieve my goals.

TABLE OF CONTENTS

LIST OF TABLES

LIST OF FIGURES

LIST OF SUBMITTED PAPERS

3D printed PCU/UHMWPE polymeric blend for artificial knee meniscus. Submitted to Tribology International. Raissa Araujo Borges, Dipankar Choudhury, Min Zou. This paper is reported in Chapters 3 and 4, and comprises the content related to the in-depth study.

Chapter 1 – INTRODUCTION

1.1. Background

Total joint arthroplasty has been a common and generally effective surgical treatment for patients suffering from arthritic disabilities, mostly due to ageing conditions or sports-related injuries. A prevalence study conducted by the Mayo Clinic estimated that 4.7 million Americans had experienced total knee arthroplasty and were carrying implants by 2014 [1]. That number was found to be nearly twice as much as the number of Americans who had been subject to total hip arthroplasty by that same year. In fact, the knee is the largest joint of the human body, yet the most vulnerable to injuries [2]. Increasing active life styles and longer life expectancy contribute to a higher rate of knee problems. A great number of those are associated with the meniscus, a cartilage cushion located between the tibia and the femur, and has a main role to absorb shocks and distribute the weight bearing across the knee joint [3]. In short, the meniscus contributes to joint stability, aids ligaments with force transmission, and provides lubrication. When injured, surgical intervention is the alternative to most cases, the patient may have the damaged part removed, but that causes changes in the cartilage load distribution, which leads to degenerative arthritis [4–6]. Results are to be improved to meet current demand of knee meniscus-related surgeries and suffice the basic joint's purpose in the human body: enable patient to walk and perform daily activities without impairment.

Yet total knee joint replacements have been in the market for at least 40 years, no artificial meniscus replacement was commercially available until the last decade [7]. The first anatomically-shaped synthetic non-anchored medial meniscus implants, NUsurface® by Active Implants, is made of a UHMWPE-reinforced PCU matrix and have been under clinical trials in the U.S. and already approved in some parts of Europe. PCU provides flexibility while the UHMWPE

reinforcement fibers promote load bearing capabilities. The solid nature of the molded implants, however, may impair the joint's ability to permit its natural lubrication mechanism to occur.

As a natural synovial joint, the lubrication in the knee is enabled by a fluid film regime that keeps the two articulating surfaces apart [3,8]. That unique tribological system has been explained by several lubrication mechanisms, which are mainly described by full fluid film lubrication, elastohydrodynamic lubrication (EHL), and micro-elastohydrodynamic lubrication (μEHL), combined depending upon the joint usage [3,8,9]. Furthermore, "weeping" lubrication happens when the joint is under dynamic load: the natural meniscus is porous and therefore absorbs interstitial synovial fluid with de-pressurization, and releases it upon loading, contributing to maintaining the opposed surfaces separated [10]. All those described mechanisms provide extremely low coefficient of friction (COF), ranging from 0.002 to 0.04 and excellent wear resistance [11,12]. In contrast to a native meniscus, there is no porosity in an artificial meniscus, which consequently makes it unable of supporting the joint lubrication via the "weeping" mechanism [9,11]. As a result, once it is implanted, the molded meniscus is only able to maintain boundary lubrication on its surface by synovial fluid absorption [3].

In this study, PCU and UHMWPE were used to explore the potential of 3D printing a blend of these two polymers for artificial meniscus implant. The peculiar layer-by-layer and line-by-line material deposition patterns of FDM 3D printing technology leave voids throughout the print, which allow the "weeping" lubrication of the knee meniscus to happen. This additive manufacturing method is versatile in fabricating different designs without needing a mold and thus can accelerate the fabrication process and facilitate the achievement of highly-customized implants suitable for individual patients.

1.2. Motivation and Objectives

The American Physical Therapy Association estimates that around 700,000 Americans undergo knee surgery due to meniscus injury every year [13,14]. Although that number seems to be surprisingly high, aside from that, there are also many people suffering from knee joint pain and that refrain from having surgery through alternative treatments. In general, knee surgery procedures are only performed when the patient has been under pain and their normal life is severely impaired due to loss of functionality of the joint. The main cause of impaired functionality and source of pain is osteoarthritis, a condition in synovial joints characterized by gradual degeneration and loss of articular cartilage. It is irreversible and consequently causes permanent damage. Before pursuing the surgery approach, patients usually undergo more conservative strategies, like pain relievers, physical therapy, and others, until being more invasive is inevitable.

The meniscus has an essential role in functioning and protecting the knee joints by dispersing contact pressure and lowering coefficient of friction. However, the most common causes of knee surgeries are meniscus-related cases [4,15–17]. Unlike replacing other components of the knee joint, such as tibia and femur, only a few options exist for meniscus-related injuries. Meniscal allograft transplantation and partial meniscus removal (meniscectomy) have been the alternative to alleviate the pain of those with meniscus cartilage damage, yet they are not permanent solutions since they ultimately lead to more medical intervention because of the uneven distribution of the pressure on the joint [18].

To fill that treatment gap, researchers have been exploring solutions for meniscus diseases, alternatives that combine long-term durability and resemble the tissue biomechanical performance. The limitations of the current options have driven research towards synthetic materials for meniscus implants. A nonanchored, polyethylene-reinforced polycarbonate urethane

meniscal implant has been under clinical trials in the USA, and in use in some countries. Those materials make this implant not only biocompatible, but also mechanically strong and capable of replicating the stress distribution in the knee. However, because the implants are molded, they lack the porosity present in natural cartilage that would provide the structure necessary to allow the knee joint lubrication mechanisms to occur. While absorption and release of synovial fluid can lubricate the porous natural meniscus, for non-porous meniscus implants only adsorption is capable of lubricating the joint [10]. This research aims to fabricate porous and mechanically robust structures for meniscus implants, combining the flexibility of PCU and load bearing capabilities of UHMWPE, by using fused deposition modeling 3D printing. That fabrication method overcomes the limitation of molding which makes only solid structures, and facilitates the implant manufacturing process by introducing practicality and the capability of easy customization. The 3D printing process is expected to provide porosity to enable synovial joint's "weeping" lubrication mechanism to occur.

1.3. Organization of the Thesis

This thesis is comprised of 5 chapters. The first and current chapter is an introductory section, bringing relevant information about knee joint implants and meniscus-related medical procedures, synovial joint lubrication basics, and the valuable significance of additive manufacturing in the biomedical industry. In Chapter 2, a collection of backgrounds of the main topics explored here are comprehended in a literature review, including a general overview of the tribology of human joints, a brief section about the history and current technologies implemented in artificial human joints, and a summary and discussion about the principles, advantages and disadvantages of 3D printing, particularly those related to fused deposition modeling. Chapter 3 details the experimental techniques used in this study, consisting of the description of the

fabrication and characterization methods. Followed by Chapter 4, which presents the results and discusses their importance, and finally, Chapter 5 draws the conclusions and makes recommendations of the direction to be targeted for future work.

Chapter 2 – LITERATURE REVIEW

2.1. Anatomy and tribology of the knee synovial joint

The knee is the largest and most complicated joint of the human body. It is classified as a synovial joint, considered one of the most important features of the human body as it serves as the core element for one's ability to move. Synovial joints are the most common in the human body and are capable of sustaining high loads and of varied ranges, yet undergoing minimal wear [19]. They also permit limited movement and are responsible for transferring forces from one bone to another [20]. All that is enabled by the mechanical properties and lubrication processes occurring within the joints. Similar to other biological environments, the surface properties such as their softness and stiffness, wettability, chemical composition, porosity and roughness are essential for the knee joints performance [21]. To understand those powerful functionalities of the knee, we will first look at knee joint's structure and operation as a synovial joint, and explore the types of lubrication mechanisms that make it a high performance bearing from an engineering standpoint.

2.1.1. Structure and surface properties of synovial joints

Figure 2.1 illustrates the parts of a synovial joint. The articular cartilage is a soft and porous material that sits on top of a hard surface, the bone. It functions as the bearing material and is essentially a compliable layer that offers excellent mechanical properties and favorable porous structure to withstand high loads permitting the lubrication mechanisms to take place. The surrounding lubricant is called synovial fluid.

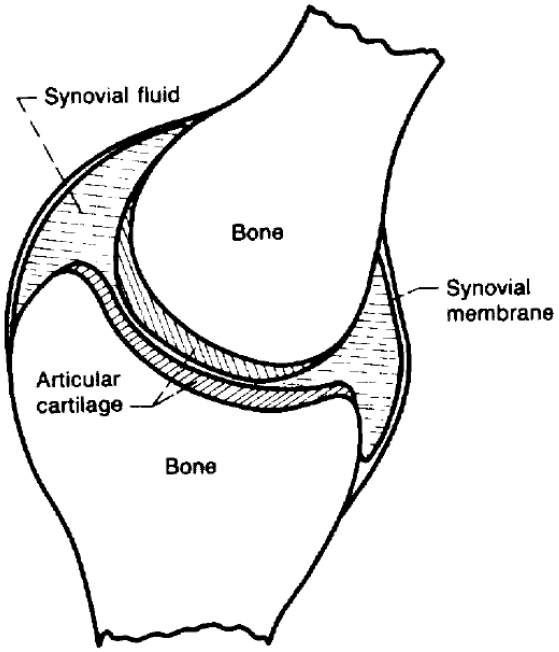

Fig. 2.1. Illustration of a synovial joint [22].

The articular cartilage layer has a thickness that depends on the kind of joint as well as the age. In general, it gets thinner as individuals age. Young and healthy individuals can have a few millimeters-thick cartilage, while the elderly may even have almost inexistent in some areas.

Due to its main function of sliding against another surface being naturally and perfectly executed, it is expected for the synovial joints cartilage to have a smooth surface. Measurements made under different studies suggest that, however, cartilage's surface roughness varies from about 1 to 5 μm [23–25]. On the other hand, healthy synovial joints can produce coefficient of frictions that are extremely low, ranging from 0.001 to 0.05, and provide exceptional wear resistance during the lifetime of the articulating surfaces [11,12,26].

The inherent porosity and elastic nature of the cartilage and meniscus tissue are the keys to the excellent tribological properties. They provide the necessary structure for the lubrication mechanisms to occur, which in turn are responsible for the superior capability of the joint to not

only sustain high loads and impacts, but also to distribute them proportionally on the knee joint throughout the gait cycle.

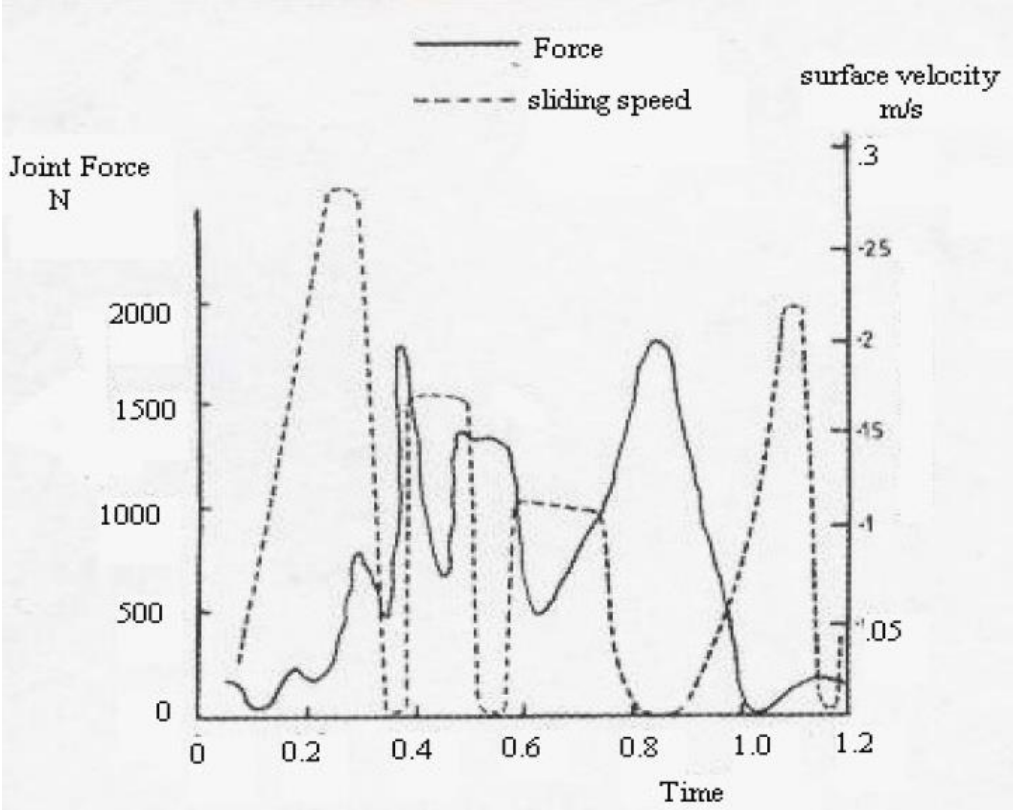

Fig. 2.2. Knee joint forces and surface velocities at different parts of the walking cycle [27].

When loads are applied on the knee joint under motion, they are not constant. Figure 2.2 shows how the applied force and the sliding velocity behave in the knee joint during a typical walking cycle [27]. The knee gait cycle is broken down into stages on Fig. 2.3. The entire cycle is categorized into stance and swing period. Those may be expressed in percentage, where the former normally constitutes 60% of the cycle and the latter 40% [9,28]. The gait cycle starts with the heel strike, the first phase of the stance period, and finishes with the terminal swing or heel strike of the same leg, the last phase of the swing period [29]. The maximum loads are about 1500 - 1750 N and is characterized by one heel striking the ground while the other foot's toes are leaving the

ground [27,30]. In Fig. 2.3 that is represented by the first phase. Sliding velocity also varies considerably with time in the walking cycle. Notice on Fig. 2.2 that when the load is high, the sliding velocity is low, and vice-versa.

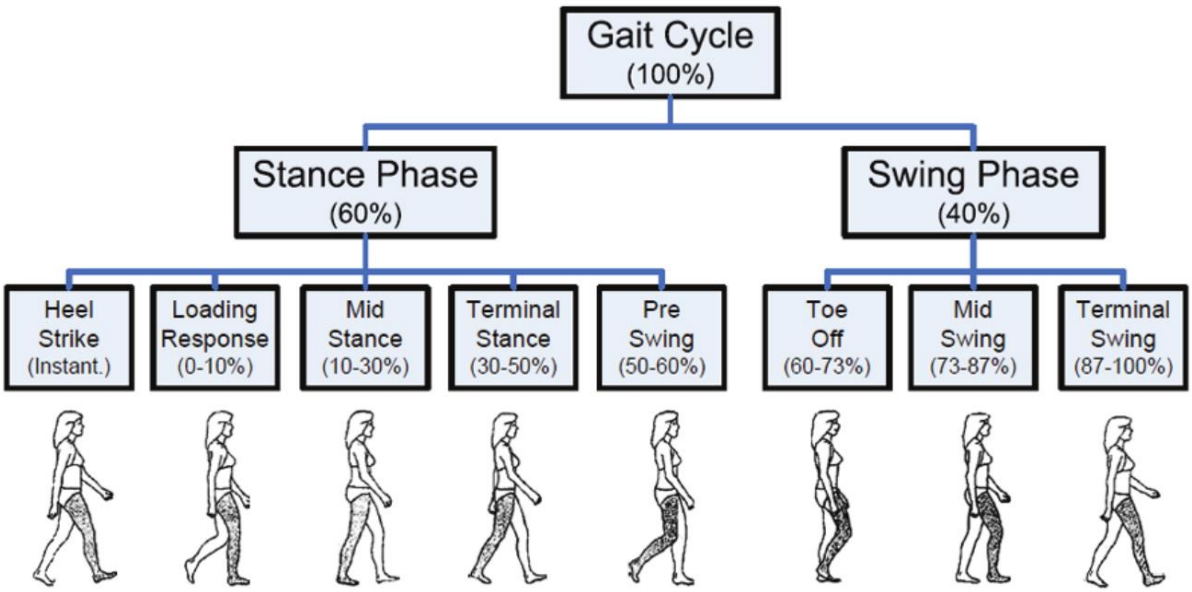

Fig. 2.3. Phases of the knee joint walking gait cycle, adapted [29].

2.1.2. The knee synovial joint structure

Three bones compose the knee joint: the femur (thigh bone), the tibia (shin bone), and the patella (kneecap). In Figure 2.4, an illustration shows that articular cartilage covers the surfaces of the tibia, femur and patella that are part of the knee joint. The articular cartilage of the knee joint is a fibrous connective tissue that is highly porous and holds a large content of water [19]. McCutchen described the articular cartilage as a bearing material that is deformable, porous and soaked with liquid [31]. Some of the major functions of articular cartilage are: distributing and transferring forces, and reducing joint friction during movement [20].

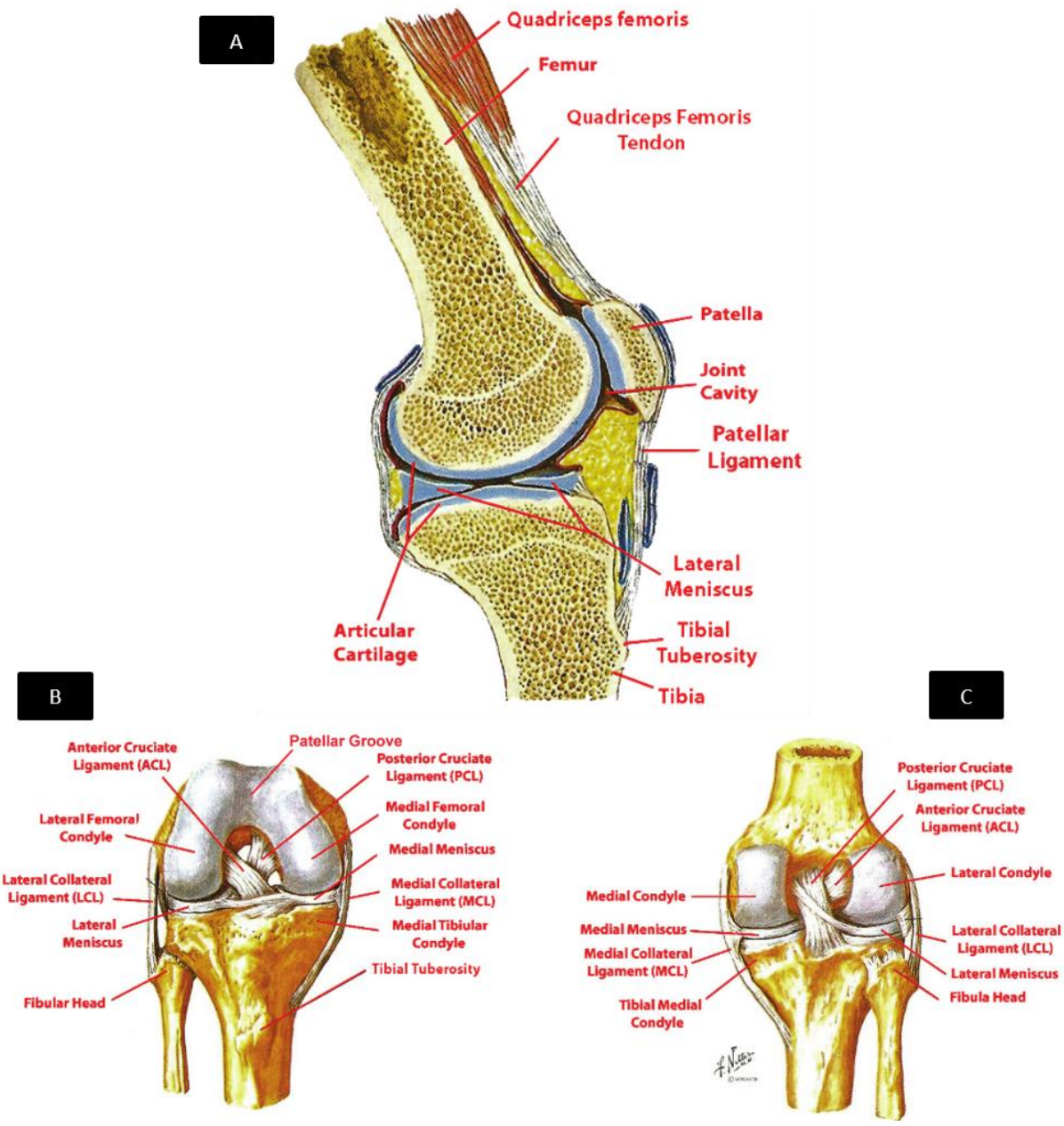

Fig. 2.4. A: Sagittal section cut of the knee joint; B: anterior view of flexed knee joint; C: posterior view of knee joint with ligaments, adapted [9]

The menisci are the two asymmetric, wedge-shaped, fibrocartilaginous discs separating the tibia and the femur, as seen on Fig. 2.4 [32]. The lateral meniscus has a circular shape and moves freely in the joint because it is only loosely connected to its surroundings. The other part is the medial meniscus, which is C-shaped and, differently from the lateral meniscus, firmly attached

to its surrounding and has restricted movement [32]. When the joint is under load, the menisci increases the contact area due the deformation of the cartilage, thus distributing the forces transmitted through the knee. It is estimated that about 40 to 60% of the compressive load applied on the knee joint is supported by the menisci [32]. A study on the contact area and pressure distribution of the tibiofemoral joint reports that, at a load of 1000 N, the menisci occupy around 70% of the total contact area of knee, and hold peak pressures of up to 3 MPa [33]. They also absorb shock and protect the articular cartilage from excessive concentrated loads, preserving it from being damaged, and cover about 70% of the knee joint contact area [33,34]. .

2.1.3. Lubrication mechanisms of the knee joint

The excellent friction and wear properties of a healthy knee joint result primarily from the actuation of the lubrication mechanisms [10,35]. A variety of lubrication processes have been described and indicated to play a role in the synovial joints, but they are mutually exclusive and have their basics on the two fundamental mechanisms of lubrication in engineering: boundary lubrication and fluid-film lubrication. Boundary lubrication happens when there is a lubricant film between the rubbing surfaces, but it is not sufficiently thick to prevent asperities contact through the film [23]. It depends on chemical properties as it is constituted of a boundary lubricant that, by molecular forces, attaches itself strongly to the solid surfaces [27]. Natural synovial joints, however, operate generally in a fluid film regime, where the two opposing surfaces are essentially separated by a fluid film [36–38].

A full-fluid-film lubrication happens when the surfaces are completely separated by a film of fluid and is considered the most effective method [27,30]. One body “floats” on a film of fluid over the pairing surface, with a very low coefficient of friction. That happens by achieving a high enough pressure in the fluid so the surfaces can be fully apart. The full-fluid-film lubrication

may be a result of liquid being pumped from outside to sustain the load (hydrostatic lubrication), or a consequence of the internal pressure generated by the rolling and sliding motion of the surfaces and the viscosity of the fluid [27]. If that generated pressure is high enough to induce elastic deformation on the bearing solids, which in turn provides greater geometrical conformity and increases the thickness of the lubricating film, then we call that elastohydrodynamic lubrication (EHL) [39]. Synovial joints rely not only on elastohydrodynamic action, but also on microelastohydrodynamic lubrication (MEHL), where the micro and nano protuberances on the surfaces of the soft bearings are partially flattened elastically by local hydrodynamic action as the load is distributed in the articulating joint [40,41]. A special case of hydrodynamic lubrication is the squeeze film, where the film remains for a certain amount of time after relative motion of the contact surfaces has stopped [9].

Weeping lubrication is a very important lubrication regime considered in this study. It was proposed by McCutchen in the early 1960's to support the idea that the interstitial fluid of the cartilage is responsible for its load bearing properties [31]. He described the articular cartilage as a bearing material that is deformable, porous and soaked with water. According to McCutchen's definition of weeping lubrication, when the cartilage is pressed, it releases the fluid from its structure through its pores to the interface, which in turn provides a fluid film support to the joint.

As the essential element in the lubrication mechanisms of the knee joint, synovial fluid is a natural lubricant that provides low friction and low wear in cartilage surfaces. It is a non-Newtonian fluid that has its viscosity effectively reduced as shear rate increases [27]. The key for synovial fluid's remarkable lubrication properties lies on the contributions of its organic constituents: proteoglycan 4 (PRG4, also known as lubricin), hyaluronic acid (HA), and surface-active phospholipids (SAPL) [35,42,43]. The fluid's viscosity appears to be governed by the

presence of HA, with the viscosity increasing almost linearly with acid concentration. It is also known that healthy joints present a more viscous synovial fluid [23,44]. Besides the organic components, albumin, a globular protein, is the most abundant protein in synovial fluid [45]. However, it is not crucial for boundary lubrication, but it has been found to decrease the wear rate of UHMWPE used in artificial joints [46,47]. When injured or in the presence of joint diseases, such as osteoarthritis and rheumatoid arthritis, the chemical environment in the joint may change, which affects cells and the secretion of the lubricant molecules by them (PRG4, HA and SAPL) [48].

2.2. Meniscus injuries and treatments

Persistent pain is usually the most important factor that motivate people to receive an artificial joint implant. Decreased range of motion is another symptom that limits patients from living a normal life. Artificial joints have been used since early nineteenth century, when infections were the most common cause of failure, and very frequently fatal [49]. It was not until the mid-twentieth century that artificial joints surgical procedures started to get more predictable and yield long lasting results. Fortunately, science and medicine have evolved to a much more reliable stage, bringing numerous different types of artificial implants in the market, covering hips, knees, intervertebral discs, etc.

Although artificial knees were developed concomitantly with hip joints, they were less successful. Inadequate surgical procedure technique was the cause for the poor results, only in the mid-1980s contemporary principles of mechanical axis balance and the concern with joint stability emerged [49]. Early in the 1970s, it was popularized the first metal-on-polyethylene condylar total knee replacement implant, completely replacing the femoral and tibial articulating surfaces [50].

The replacement the entire joint became common practice among patients with persistent pain due to degenerative arthritis. Figure 2.5 shows the great increase of cases treated by total knee replacement between 2000 and 2010 [51].

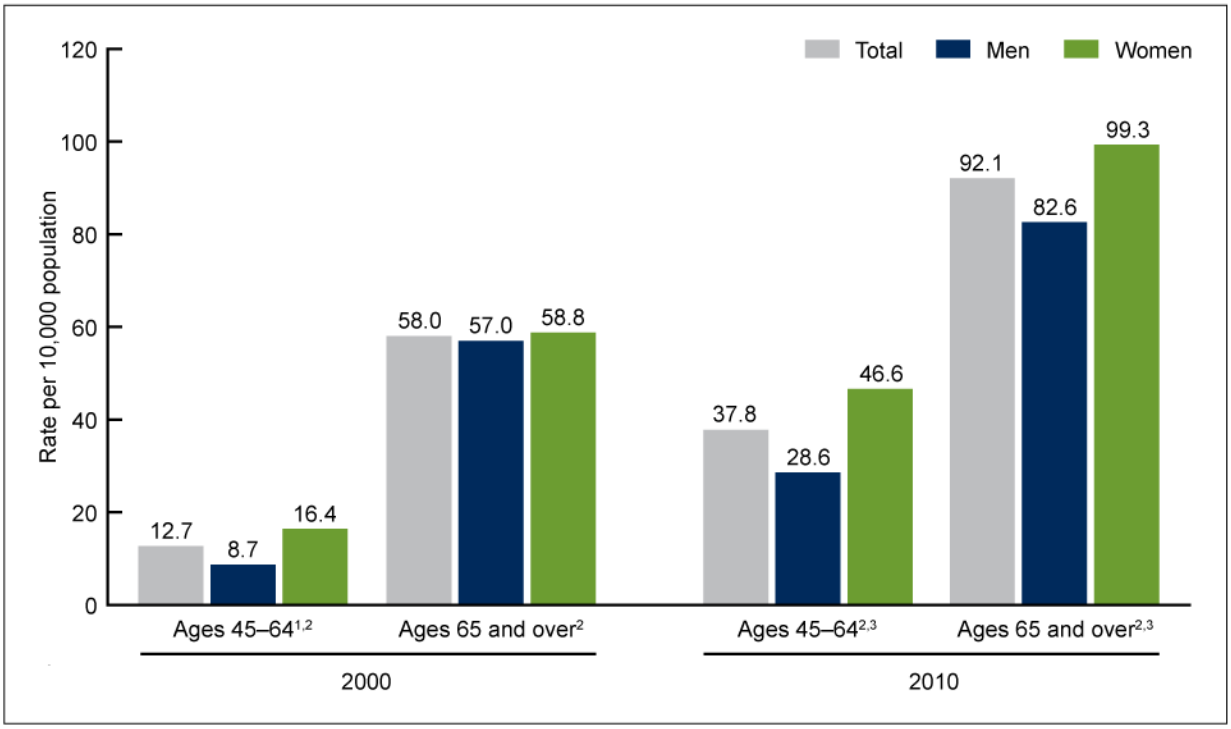

[1]Significant difference in 2000 between men and women within age group ($p < 0.05$).
[2]Significant difference between 2000 and 2010 within sex and age group ($p < 0.05$).
[3]Significant difference in 2010 between men and women within age group ($p < 0.05$).
NOTES: Total knee replacement is defined as code 81.54 of the *International Classification of Diseases, Ninth Revision, Clinical Modification* (ICD–9–CM) for any of four collected procedures. Rates were calculated using U.S. Census Bureau 2000-based postcensal civilian population estimates.
SOURCE: CDC/NCHS, National Hospital Discharge Survey, 2000 and 2010.

Fig. 2.5. Total knee replacement among inpatients aged 45 and over, by sex and age group: United States, 2000 and 2010 [51].

When it comes to meniscus, historically, it was believed for many years that the menisci were vestigial remnants of leg muscles, and that their removal (total meniscectomy) was considered beneficial in cases of torn meniscus treatment because of the instantaneous disappearance of impairment and pain. [2,52]. The importance of the meniscus in load bearing and distribution was only elucidated around the 1970s and 1980s, when studies showed that the contact stresses on the tibial plateau increased proportionally with the amount of meniscus tissue removed [53,54].

In general, approximately 85% of the cases of meniscal tears require surgical intervention compared to other knee-related injuries [17]. Depending on the case, meniscus tears may be more or less difficult to treat. Sutures, staples, and anchors are repairing strategies that tend to preserve the tissue, but that only successfully heal the torn meniscus if the damage is located in the vascularized region [55]. Otherwise, lesions are irreversible and patients are recommended to undergo partial meniscectomy, which consists in removing the affected region of the meniscus. However, the partial loss of the meniscus lead to degenerative arthritis because of cartilage unbalanced load distribution [4]. That results in post-meniscectomy pain and further medical intervention. Patients younger than about 50 years old are usually suggested to remain under more conservative approaches, such as medication, injection of HA, knee brace, physical therapy, limitation of physical activities, or undergo another partial meniscectomy (sometimes followed by other meniscectomies) [18]. In more severe cases, or in a more advanced age, a meniscal substitute is indicated.

Nowadays, meniscus replacement is still considered an unsolved problem in orthopedics [18]. The current treatment for symptomatic post-meniscectomy patients is a meniscal allograft transplantation. Although it relieves pain and improves knee function, the procedure is not only risky, involving probability of disease transmission, but it is also of difficult availability. It is hard to find allografts with appropriate sizing of the recipient: oversized allografts can increase the forces across the articular joint, and undersized can lead to excessive load and poor congruity with the bones [3,18,56]. Furthermore, another drawback is that allograft meniscus undergo remodeling after being implanted, which causes shrinkage of the implant and impacts the joint's mechanical strength [3,18]. Biodegradable options exist, polymeric synthetic and natural prostheses are made of temporary scaffolds that gradually degrade in the body, giving place to a newly formed tissue.

However, that path may be limited due to the absence of durability associated with most of the biodegradable materials when *in vivo* conditions and unpredictable variability of body response to the implant [57]. Besides, there is little evidence about its effectiveness, or whether a meniscus allograft would reduce the risk of osteoarthritis progress [58,59]. The table below summarizes the current alternatives for treatment of meniscus injuries, from conservative approaches to invasive choices being practiced around the world.

Table 2.1. Knee meniscus treatment alternatives.

	Available meniscus injury treatments	**Description**
Non-invasive / minimally invasive	Physical therapy	An alternative to decrease swelling and relief pain, it is commonly combined with compression and pain medication. Physical therapy works on strengthening the knee and leg muscle to improve patient's mobility. It reliefs the pain but it doesn't heal the injury.
	Injections	Cortisone and hyaluronic acid injections help reduce inflammation by improving the knee joint lubrication. This is also a temporary relief.
	Stem-cell therapy	Injection of patient's own stem cells into the knee joint, where they differentiate and may help healing the meniscus. This treatment is costly and still considered experimental, there is no long-term understanding of its effects.
Surgical	Meniscectomy	Removal of injured part of the meniscus. This is a very common procedure, but that leads to maldistribution of the pressure on the knee joint. Consequently, further degeneration of cartilage happens, causing osteoarthritis, pain and discomfort. That is the cause of future meniscectomies and ultimately a total meniscus removal, asking for more radical treatment options.
	Meniscus allograft	Transplantation of part of the meniscus from a donor. Associated with risks of infections and rejection of the transplant, and is also very difficult to find a matching option.
	Partial meniscus implant	There are currently two options for partial meniscus substitutes. The Menaflex®, or Collagen Meniscus

		Implant (CMI) is a porous scaffold made of fibers from bovine Achilles tendon collagen [60]. The Actifit® is also a porous scaffold, but made of synthetic polyurethanes with semi-degradable stiff segments and biodegradable polyester [61]. Both Menaflex® and Actifit® were designed to promote tissue growth and regeneration and stimulate healing the meniscus tissue [60]. There are not enough evidences of their efficacy and the FDA has not cleared either option, although they have received CE marking in some parts of Europe.
	Total knee replacement	This is the most radical approach, since it replaces the entire knee joint with an artificial joint. Usually made of two articulating surfaces of titanium and Co-Cr, attached to the bones, and an UHMWPE spacer between them. Although this has been a common procedure for decades, it fails mainly due to wear of the polyethylene, inducing osteoarthritis [62].
	Artificial total meniscus implant	A molded polycarbonate urethane total meniscus implant was developed in the last decade. Its structure is made of a PCU matrix and UHMWPE fibers and resembles the natural joint, that has a solid matrix and oriented collagen fibers [18]. It has been under clinical trials in the U.S. and received CE marking in Europe.

Recently, a synthetic non-anchored medial meniscus implant has become an alternative to those middle-aged patients to delay more aggressive treatments. The NUsurface® meniscus implant (Active Implants Cop., Memphis, TN) is a free-floating PCU meniscal implant, reinforced circumferentially with UHMWPE fibers, and currently under clinical trials in the United States. Its design was optimized with finite element modeling of the material and the resultant contact mechanics on the tibial articular cartilage [7]. Its structure, composed of a PCU matrix with surrounding polyethylene fibers, aims to mimic functionality and structural components of the natural meniscus, made of a sound matrix with highly oriented collagen fibers [63,64].

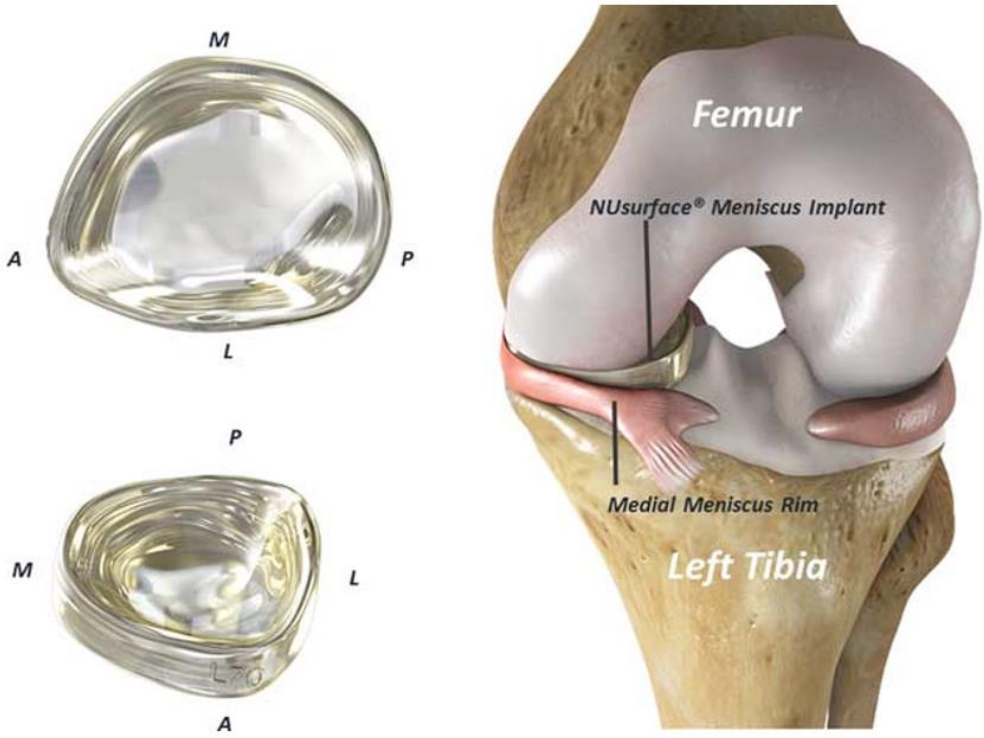

Fig. 2.6. NUsurface® Meniscus Implant [18].

The NUsurface® has shown potential safe use in animal models, matching cartilage condition with control joints for up to six months after implantation [65]. Good load transfer and distribution capabilities were observed in vitro using human cadaveric knees [66]. Figure 2.7 shows the medial (M) and lateral (L) tibial plateau in different conditions: upper left is the natural state, partial of meniscectomy of the medial meniscus on the upper right, another meniscectomy of the medial (subtotal) in the lower right, and following implantation of NUsurface® in the lower left [18]. A follow-up study of 3 patients implanted with the NUsurface® implant reported that the knee preserved its static kinematic properties after surgery [67].

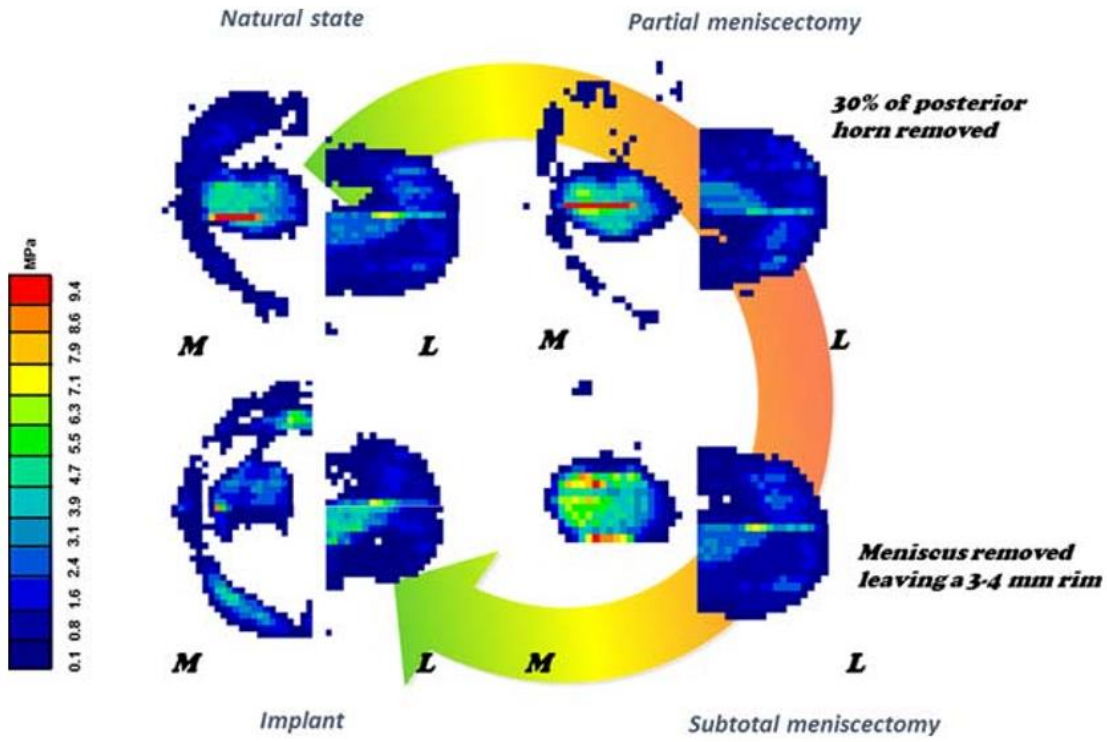

Fig. 2.7. Pressure distribution maps in the meniscus after meniscectomy and following NUsurface® implantation [18].

PCU is a polymer that has emerged as a result of the interest, within the biomedical industry, in developing biocompatible, biostable, synthetic materials for the replacement of soft load-bearing tissues, like meniscus, articular cartilage, and intervertebral disc. As an individual ages, those tissues tend to degenerate, significantly impairing their lives [68,69]. Thus, finding a synthetic material that resembles cartilage in terms of mechanical properties and wear resistance is of high importance. Below are reported the moduli of elasticity of different materials that have been studied for human bearing applications, compared to that of natural cartilage of the knee.

Table 2.2. Materials used in human bearings applications. Adapted from Miller [70].

Material	Modulus of elasticity (MPa)
Co-Cr alloys	200,000-253,000
Titanium alloys	110,000-115,000
Stainless steel (316)	190,000-200,000
UHMWPE	800-1,600
PCU (75A-95A)	12-42
PDMS	3
Articular cartilage	2-45

Molded UHMWPE has been commonly used for joints implants for many years. In the case of total knee joint replacement, since the mid twentieth century, with improvements being made throughout the years [71]. However, despite the efforts, it ultimately results in releasing wear debris, causing premature failure of the implant. Although UHMWPE is biocompatible in its bulk form, wear debris from the polymer has been found to trigger osteolysis in surrounding tissues, which leads to implant loosening and eventual implant replacement surgery [72]. Furthermore, the rigid and solid nature of the mold hinders joint's native lubrication mechanisms. Therefore, research has aimed the direction of more compliant materials that not only have mechanical properties like articular cartilage, but that would also stimulate lubrication and have a more realistic load distribution in the joint. The biggest concern among clinicians is the wear behavior of any new or novel bearing material. Their target is to have wear debris minimized and therefore prevent osteolytic lesions of artificial implants [73].

A study has found that the elastomeric polyurethane Pellethane® 236380A can achieve lower wear rates than UHMWPE in a simulated in vivo wear environment [74]. They reported the reason for the higher wear resistance to be due to the compliance of the elastomer and its ability to conform to the geometry of the counterface, causing reduction in contact pressure. Other soft polymers have been investigated for implant materials. Silicone (PDMS), for instance, was

considered potentially suitable for artificial replacement of joints until the late 1990's, until it was found to fail due to different reasons, including fracture, compressive deformation, inflammation, and foreign body response. The table below

2.3. Fused Deposition Modeling

In the past few decades, additive manufacturing has introduced a nearly complexity – free and highly customizable era into the manufacturing industry [75]. Since the advent of the first method, Selective Laser Sintering, several other technologies have been developed, expanding materials usage flexibility and enabling increasingly competitiveness in that market. Among the seven types of additive manufacturing methods, fused deposition modeling, or FDM, is probably the most diffused kind due to its accessibility and ease of use. Developed and patented by Stratasys (Eden Prairie, MN) more than 20 years ago, this technology is relatively simple and affordable when compared to other additive manufacturing processes, characteristics that have taken FDM beyond conventional industry's boundaries [76]. FDM's versatility to fabricate prototypes, tooling accessories, and functional parts straight from a virtual model and its capability of realizing those parts without geometrical complexity limitations have enabled increasing popularity in a wide array of fields [77]. In the biomedical field, FDM have contributed to a variety of applications, such as tissue engineering, implant fabrication, dental solutions, drug release, and medical equipment fabrication [78–82].

FDM technology working principles rely especially on thermodynamics and mechanics of materials: it works by heating up a thermoplastic filament to make it malleable and extrude it through a nozzle, which in turn, deposits the solidifying polymer layer-by-layer on a tray or base member (also called print bed) [83]. To promote attachment, the print bed can be heated. The bonding between layers is promoted by the diffusion bonding mechanism, driven by the thermal

energy of semi-molten material [84]. The movement of the dispensing head relative to the base follows a predetermined pattern along the axes (“x”, “y”, and “z”) in rectangular coordinates. When the first layer is finished, the print bed is lowered by a fixed distance (i.e., the thickness of a single layer), and a second layer can be printed on top of the original one. By repeating these steps, an object is created in an additive manner.

The 3D object is designed digitally using a computer-aided design (CAD) software and converted into multiple-layer data, known as G-code, by a commercially available software. Then, it is imported through drive signals into a computer-aided machine controller to the drive motors.

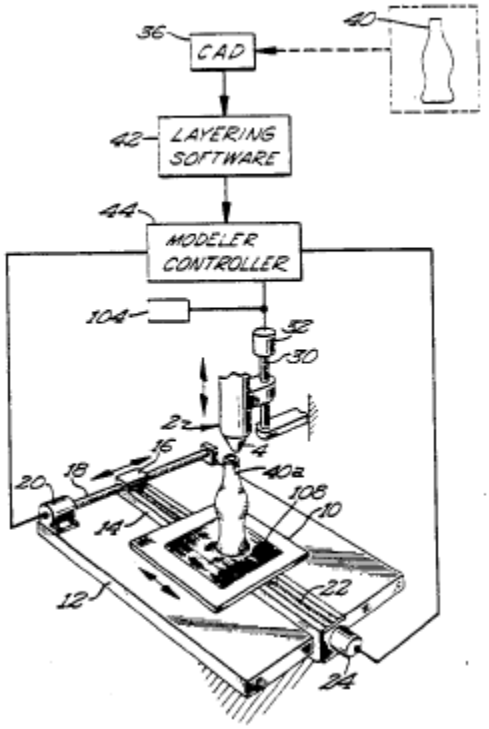

Fig. 2.8. FDM original schematic [83]

The material is provided in the form of a spooled filament and is fed into a liquefier head through the use of computer-driven counter-rotating rollers [85]. The head is maintained at a certain temperature in order to soften and melt the filament just above its melting point. The head

is computer-controlled to move in the horizontal plane, while the build platform supplies the vertical motion. The deposited material, in the form of a thread, lays down on the bed, and was referred to as "road" when related to Stratasys first FDM machines [86]. The extrusion and deposition processes utilize as principle a constant volumetric displacement profile. Thus, material flow rate, which is controlled by the speed of counter-rotating rollers, determines the dimensions of the deposited "roads" [87].

According to Mukesh K. Agarwala et al., FDM process parameters can be categorized into four types: operation specific parameters, machine specific parameters, materials specific parameters, and geometry specific parameters [86]. The table below lists the process variables into those four categories. Parameters are interdependent and should be considered together when planning a print.

Table 2.3. FDM process variables, adapted from [86].

Operation Specific	Machine specific	Materials specific	Geometry specific
Slice thickness	Nozzle diameter	Powder characteristic	Fill vector length
Road width	Filament feed rate	Viscosity	Support structure
Head speed	Roller speed	Stiffness	
Extrusion temperature	Flow rate	Flexibility	
Fill pattern	Filament diameter	Thermal Conductivity	

Operation specific parameters are the ones defined in the steps prior to printing; they are crucial to the build good quality and depend on what is chosen by the user in the slicing phase. Road width and thickness, as well as the print-head speed, define the flow rate of the material to be extruded out of the nozzle. On the other hand, resolution of the deposited material is dependent on the distance of the nozzle to the bed. In other words, the thickness of the thread (usually between 0.1 and 0.3 mm) is controlled by two factors: the distance between the nozzle and the print bed and the ratio between the flow rate of the filament through the nozzle and the printing speed [88].

Originally limited to proprietary materials when released, FDM technology now supports a much broader list of materials. However, they should have low melting temperatures and rapidly solidify with minimum residue stress or distortion upon adhering to the previous layer [83,89]. Viscosity of the material at the extruding temperature should be high enough to form well-defined "roads" but, at the same time, low enough to allow proper extruding through the nozzle. Thermoplastics have been the material of choice for FDM, with the most common being acrylonitrile butadiene styrene (ABS), polycarbonate (PC), polylactide (PLA), polyamide (PA), and the combination of any two different thermoplastic materials [90–92]. Functional agents, namely metal particles, carbon nanotubes, and graphene, are often blended with thermoplastics for tailoring properties that enhance the resulting material's performance [93].

Recently, 3D printing of PCU has been accomplished by Miller et al., who have explored mechanical properties of the printed structures, particularly focusing on fatigue and cyclic efforts [94]. Besides that, they also studied how the printed architecture affects the mechanical properties and fatigue performance of polyurethanes [70]. It was found that PCU, under cyclic compression tests, present superior energy dissipation capability compared to other tested soft polymers (silicone and acrylate), and that mechanism was found to be enough for PCU to outperform and resist fatigue fracture. Furthermore, it was observed that 3D printed samples matched or exceeded injection molded samples in terms of monotonic tension, compression, shear, and tensile fatigue. By comparing different printing internal structure architectures (or print infill geometries) they also concluded that the fatigue performance of PCU is not significantly affected by the inclusion of such architectures, as opposed to stiffer materials. That is attributed to the versatility and compliance of soft polyurethanes, and reinforces the benefits of using 3D printed PCU for artificial meniscus implants.

Rocha et al. emphasized the scarcity of studies about printable polymer blends in literature, and developed an ABS-based polymeric blend containing ABS, UHMWPE, and a compatibilizer, styrene ethylene butadiene styrene (SEBS) [95]. They fabricated different weight concentrations of the blend, performed tensile tests and measured roughness of printed surfaces. More importantly, they demonstrated the ability of creating printable polymeric blends that can tailor physical properties and be customized for a given application. ABS was also used by Torrado et al. as matrix for polymeric blends and composites [96]. Recently, efforts in fabricating UHMWPE-based 3D printing filament have been made by Ansari et al., who used hydroxyapatite as a filler to reduce UHMWPE viscosity [97]. Despite the successful 3D printing of ABS polymeric blends as well as PCU and other thermoplastic urethanes, there is no reported literature about using FDM to 3D print blends of UHMWPE and PCU. This work presents the fabrication of novel PCU/UHMWPE polymeric blends for FDM 3D printing and explores their tribological performance for knee joint applications.

Chapter 3 – EXPERIMENTAL METHODS

3.1. Sample fabrication

3.1.1. Filament fabrication

Polycarbonate urethane was acquired in the form of resin pellets from two vendors: Bionate II 90A from DSM (Exton, PA), and Chronoflex C 93A from AdvanSource Biomaterials (Wilmington, MA, USA). A biocompatible grade of UHMWPE pellets was purchased from Ticona Polymers Ltd (Florence, KY), and blended with each type of PCU in 5 and 10, and 15% weight concentrations. It has been found that the addition of 10% wt. of UHMWPE into PCU may improve the wear resistance of the matrix, as well as that performance can be significantly reduced by increasing the concentration of UHMWPE to 20% wt. [98].

Preliminary studies were done with Ninjaflex (Ninjatek, Manheim, PA), Bionate and Chronoflex to find the best set of print parameters, and the advantages and difficulties in the processing and testing each of them. In that preparatory phase, all the mentioned concentrations of UHMWPE were used (5, 10, and 15% wt.) to blend into Bionate and Chronoflex and investigate if it was possible to carry out 3D printing with UHMWPE considering it cannot be extruded using conventional extrusion methods. Ninjaflex filament, on the other hand, was obtained to investigate the best parameters and configurations during 3D printing. Although it is also another kind of thermoplastic urethane, that polymer is not appropriate for biomedical application, but only for household used.

Further investigation and characterization were conducted with Chronoflex and UHMWPE, in which 3D printed, as well as compression molded samples were analyzed more in depth than the preliminary study previously mentioned. For that, pure Chronoflex (CF) samples were both molded and 3D printed, while UHMWPE was only compression molded since it cannot

be 3D printed. The nearly zero melt-flow index of UHMWPE makes it not suitable for extrusion-based processes [99,100]. The 10% wt. of UHMWPE in PCU (PCU/UHMWPE blend) was chosen based on results found in literature [98], and considering that the extrusion of that concentration presented fairly consistent results, different from concentrations above 10%.

In order to minimize the moisture content, all the resins were subject to a drying process in a vacuum oven (Fisher Isotemp Vacuum Oven Model 282) for 10-13 hours at 100 °C. When moisture is present in the material to be extruded, the filament produced is not continuous, causing, bubbles, gaps and air voids throughout the filament, which are defects that can be carried through the 3D printing [101]. For the same reason, the pellets, filaments, and the 3D printed samples were maintained in a nitrogen desiccator at all moments when not in use.

The following table shows the types of blends and their respective identification names used as reference in this research.

Table 3.1. PCU (Chronoflex and Bionate) and UHMWPE blends.

Polymer Base	Sample ID	PCU wt. %	UHMWPE wt.%	Filament Extrusion Temperature
Chronoflex	CF0	100	0	183 °C
	CF5	95	5	
	CF10	90	10	187 °C
	CF15	85	15	
	CFm	100	0	183 °C
Bionate	BN0	100	0	186 °C
	BN5	95	5	
	BN10	90	10	190 °C
	BN15	85	15	
UHMWPE	UHMWPEm	0	100	N/A

Filament fabrication process was carried out using a Filabot EX2 (Filabot, Barre, VT), a single-screw desktop filament extruder and following manufacturers' suggestions of processing temperature range. Table 3.1 summarizes the temperatures used to extrude the 2.85 mm filaments. To promote cooling, a fan was placed 50 cm from the extruder nozzle. Figure 3.1 shows the Filabot EX2 extruding a segment of filament.

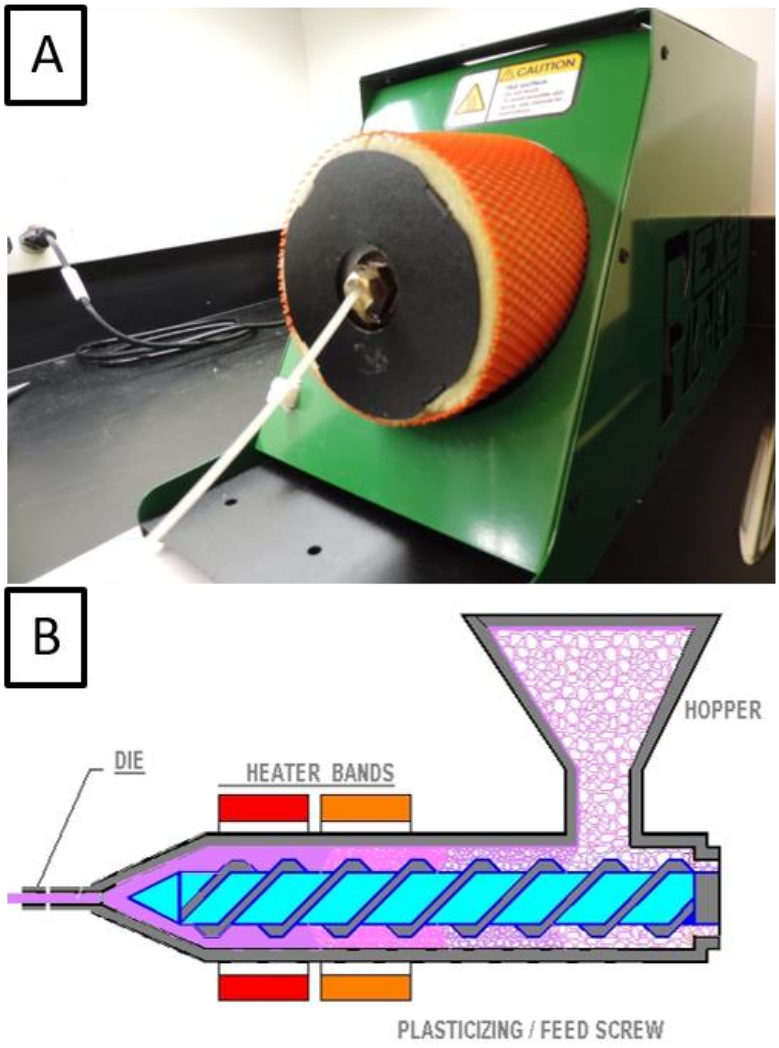

Fig. 3.1. (A) Filabot EX2 used to fabricated the filaments for 3D printing. (B) Schematic showing the internal part of a single screw filament extruder [102].

3.1.2. 3D printing

An FDM 3D printer, was used to fabricate the samples: a Lulzbot TAZ 6 with a FlexyDually V2 print head (both from Aleph Objects, Inc., Loveland, CO), customized with a 0.25 mm brass nozzle (E3D, Oxfordshire, United Kingdom). Ninjaflex filament was used to investigate the best set of 3D printing parameters that produced the best processing performance and sample quality.

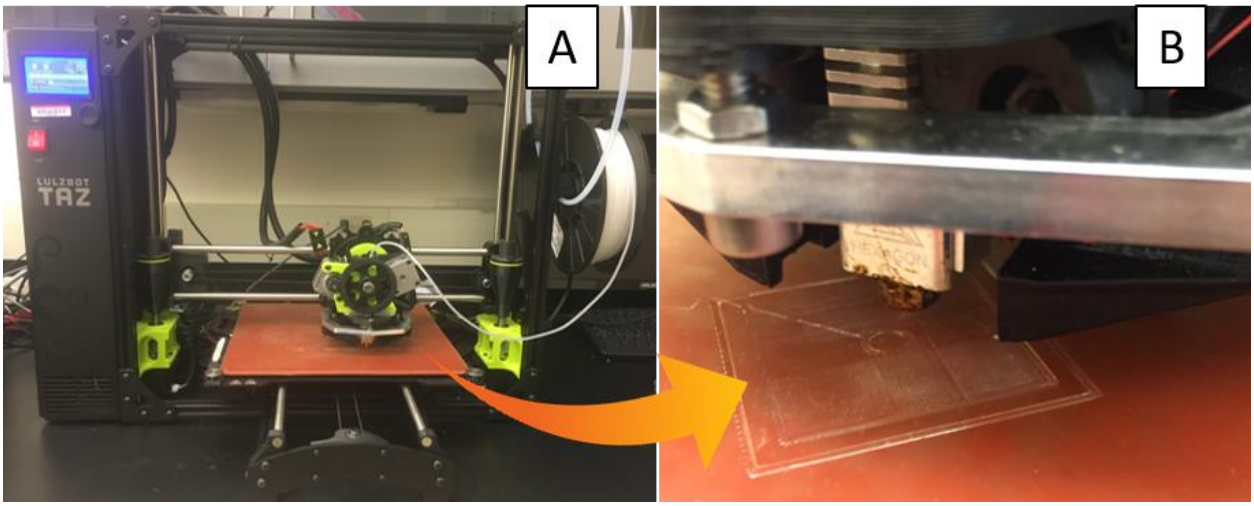

Fig. 3.2. (A) Lulzbot TAZ 6 printing a sample and (B) a closeup image of its nozzle.

All samples were printed on a polyetherimide print bed at 50 °C and with the nozzle temperature set at 225 – 235 °C. Print infill had 100% density using a 0.125 mm layer height, and following a rectilinear pattern, which was explored in the preliminary study. Speed throughout the print job was 20 mm/s, while a reduced speed of 15 mm/s was maintained for the bottom and top 4 layers to ensure an improved surface finish. The FDM samples were designed using Solidworks and measured 32 mm × 32 mm × 3 mm. Cura, a 3D model to toolpath slicer software for Lulzbot, was used to slice the models and generate the G-code. The bottom of the 3D printed samples that is in contact with the print bed was used for tribology tests because of its smoother surface.

Compression molded samples had a diameter of 38 mm and a thickness of 5.3-5.4 mm and were not subject to any surface treatment after molding.

3.2. Sample characterization

The following set of characterization measurements was performed along with the in-depth study. Therefore, their description does not apply for the preliminary study.

A laser scanning confocal microscope (LSCM, VK-X260K, Keyence, USA) was used to measure the average surface roughness (S_a) and root mean square roughness (S_q), and to visualize the wear tracks after the tribology tests. Analysis and measurement of wear track depth and cross-sectional area were performed with Keyence's Multi-File Analyzer software.

X-ray diffraction (XRD) measurements were performed on clean samples to examine the crystallinity after blending and fabrication. These measurements were carried out using a PW3040 X'Pert-MPD (Philips, Holland) diffractometer with Cu Kα-radiation, $\lambda = 0.15418$ nm, in Bragg–Brentano geometry [103].

A video-based contact angle measurement system (OCA 15 plus, DataPhysics Instruments GmbH, Germany) was used to measure the water contact angles (WCAs) of the samples through the sessile drop method. Three measurements were taken across the surface of each sample using de-ionized water droplets of 3 µL. An average of left and right contact angle was calculated for each of the measurements.

Absorption tests were conducted by immersing samples in a 30 vol. % solution of bovine serum in water, refrigerated at 4-6 ºC. The samples were dried in a vacuum oven at 100 ºC for 10-12 hours prior to the procedure. They were then subject to complete submersion for 24 hours, during which they had their weight checked at 10, 20 and 40 minutes, and every hour for the first 6 hours, followed by checkpoints at 12 and 24 hours. At each inspection, samples were

removed from media, blotted dry, and immediately weighted on a precision balance (GD-503-NTEP, Sartorius, Germany).

To observe the internal structure of the 3D printed samples, microtome technique (IsoMet Low Speed Saw, Buehler, Lake Bluff, IL) was used for cutting and scanning electron microscopy (SEM; model XL-30, Phillips/FEI, Hillsboro, OR) was used for visualizing the cross-sectional area.

3.3. Tribological testing

A Universal Mechanical Tester (UMT-2, Bruker Corporation, San Jose, CA, USA) was used to perform the tribological tests. The machine measures simultaneously frictional forces and normal loads, and for this experiment, it was equipped with a temperature controlled chamber, where a custom lubricant and sample holder were assembled and maintained. A variety of rotational oscillating tests was performed, varying the sample analyzed, duration of the test, lubricant, applied load, counterface, and oscillation angle. An oscillation angle between 32.4° and 39° and a speed of approximately 7.33 mm/sec were maintained, while the temperature chamber preserved the environment at 37° C. Three series of friction tests were performed using different materials:

1- Ninjaflex and 6.35 mm S_3N_4 balls;
2- 3D printed Bionate and Chronoflex (two PCU types), 3D printed PCU/UHMWPE blend, and 6.35 mm S_3N_4 balls;
3- Molded Chronoflex, UHMWPE, and 9.5 mm S_3N_4 balls.

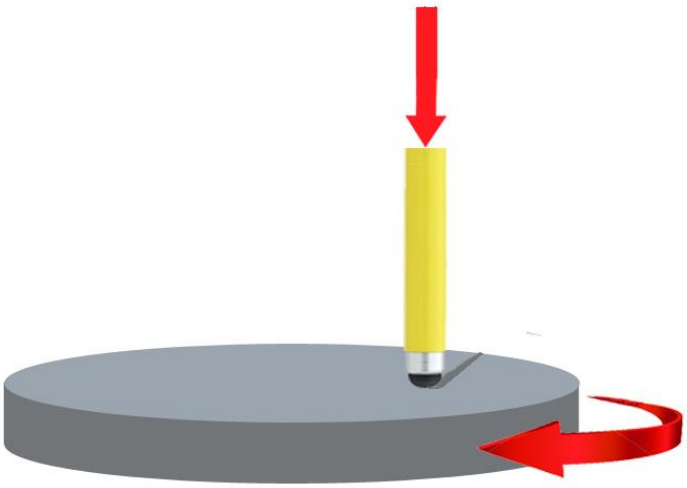

Fig.3.3. Schematic of rotational oscillating test. Stage has sample attached and rotates at a specific speed. The load is applied by the counterface, which stays constant.

A first set of tests was conducted on samples made of Ninjaflex with the objective of evaluating the coefficient of friction of 3D printed samples using two orientations. The rectilinear pattern was adopted, but the samples were placed in different positions relative to the pattern followed by the printer algorithm. A photo of the samples can be seen in Fig. 3.4. These friction tests lasted for 30 minutes and the samples were subject to 2N and 5N loads in each test, applied by a 6.35 mm silicon nitride ball. Contact pressures generated were 1.9 MPa and 2.6 MPa, calculated with properties supplied by the manufacturer and from a study made by a research group in Finland [104,105]. The loads were chosen to create stresses within the range that is transferred to the meniscus, reported on literature [33]. Only one sample of each kind was tested. Medium was deionized water at 37 °C and oscillation angle was 39°.

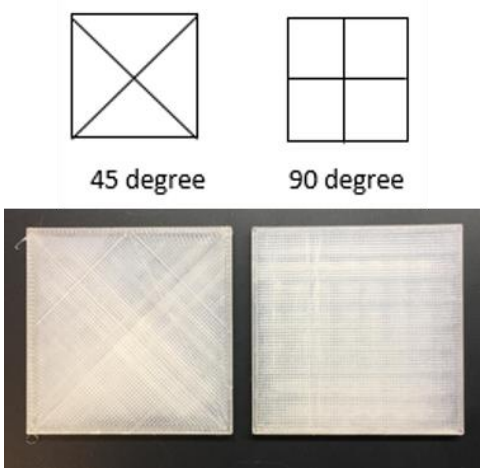

Fig. 3.4. Schematic and photo illustrating the two different printing orientations adopted in the preliminary study.

Upon choosing the print orientation, a second series of preliminary tests was conducted, now using Chronoflex and Bionate, as well as their blends with UHMWPE. The goal was to compare the performances of both types of PCU throughout the entire fabrication process, until evaluation of friction tests. Counterface was a Si_3N_4 ball with 6.35 mm diameter and loads of 2 and 5 N were applied for a total duration of 2 hours, resulting in contact pressures of 1.7 and 2.4 MPa, respectively.

As a preliminary set of tests, these were run only once per each type of sample under the each of tested loads. From this point on, the knee joint environment was replicated by testing the sample immersed in a 30 vol. % solution of bovine serum in water, which was prepared by stirring the solution on a magnetic plate for 5 min at 500 RPM.

For the in-depth study, 3D printed and molded samples were subject to 8-hour long tests, rubbing against a 9.5 mm Si_3N_4 ball. A normal load of 11.5 N was applied, which generated a maximum contact pressure of 45.2 MPa on the molded UHMWPE. That is about twice the recommended initial peak Hertzian contact pressure according to ASTM F732 for standard test method for total joint prostheses [106,107]. The same normal load was applied on pure PCU and

the 3D printed blended samples, which resulted in a maximum Hertzian contact pressure of 2.4 MPa for the former.

Prior to undergoing any characterization and tribological experiments, the samples were cleaned according to the cleaning procedure described on Annex 1 of ASTM 2025. Table 3 shows the details for the friction tests, and Fig. 3.5 shows the UMT-2 in a detailed image of the experimental setup, with a 3D printed sample clamped in the sample holder.

Table 3.2. Tribological experiment details relative to preliminary tests with Bionate and Chronoflex, as well as in-depth investigation.

Material	Ball Diameter (mm)	Load (N)	Max. Hertzian Contact Pressure (MPa)	Max. Hertzian Contact Pressure (MPa) ASTM F732	Rotational Speed (RPM)	Equivalent Linear Speed (mm/sec)	Oscillation Angle	Temperature
PCU	6.35	2	1.7	29-36	10	7.33	36 °	37 °C
		5	2.4					
	9.5	11.5	2.4					
UHMWPE	6.35	2	33					
		5	44.8					
	9.5	11.5	45.2					

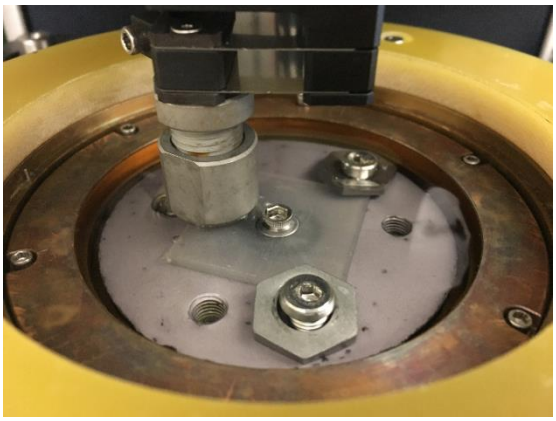

Fig. 3.5. Tribological experiment setup: Sample immersed in bovine serum solution in UMT-2 chamber (37^0 C).

3.4. Statistical analysis

The results were statistically analyzed using un-paired, two-tailed Student's t-test with $p \leq 0.05$ as threshold for significant differences between groups. All experiments from the in-depth study were performed at least 3 times. Figures in the results were judged the best representative of all samples, and all graphs represent averaged results of experiments run on all the samples, when applicable.

Chapter 4 – RESULTS AND DISCUSSION

4.1. Preliminary study

Figure 4.1 shows the results of the study run on Ninjaflex to understand whether print orientation affected tribological properties of the 3D printed samples. Only the curve representing Ninjaflex printed at 90° under 5N load appears to approach stabilization within the first 30 minutes of testing. Between the 2N tests, the result of the same sample, NF90, also showed a curve that had a smaller inclination, and therefore reaching a steady state faster than NF45. Thus, a 90° print orientation was used for the following 3D printed samples.

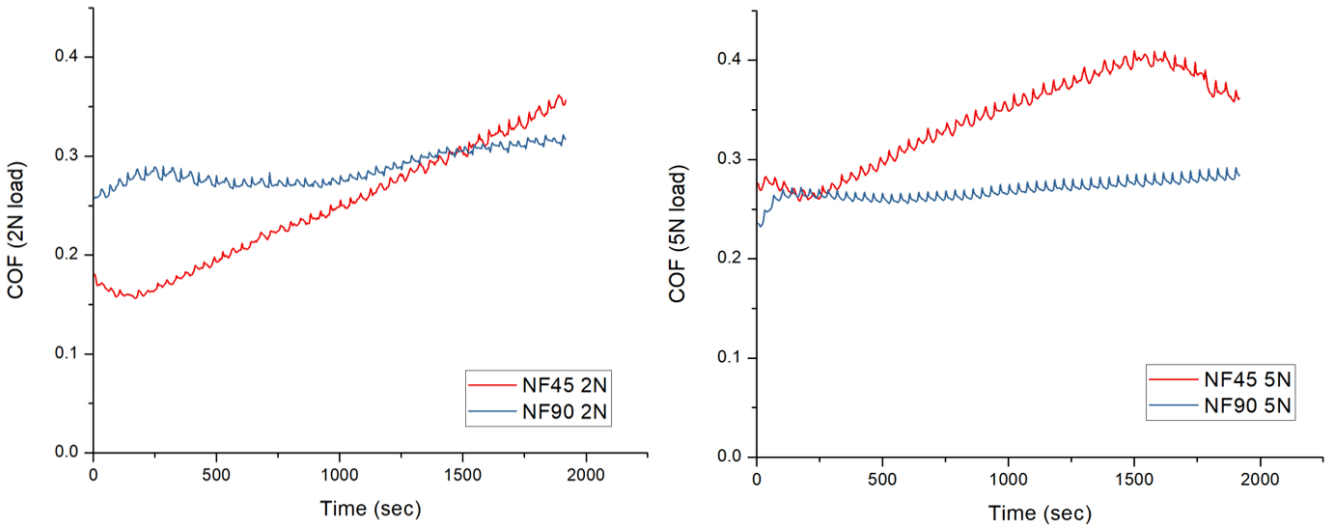

Fig. 4.1. COF curves for 2 and 5N friction tests on Ninjaflex printed with different orientations.

The 2-hour friction tests results are summarized on fig. 4.2, which shows the average COF of each sample under 2 and 5 N loads. The biggest take away here is that it is feasible to 3D print PCU with small quantities of UHMWPE, despite the nearly zero melt flow index of UHMWPE. Extrusion became less consistent as the UHMWPE quantity increased and the flow rate fluctuated considerably with the 15% wt. blends.

In general, Bionate samples presented a higher COF compared to Chronoflex with the same UHMWPE concentration and under the same testing conditions. Furthermore, it is noticeable that friction seems to decrease with the addition of UHMWPE, reinforcing the hypothesis that UHMWPE helps supporting the load because of its strength. It was decided to pursue the next steps using only Chronoflex and the 10% blend of PCU/UHMWPE due to its better performance and results from the sample fabrication process. The extrusion of the blends got more difficult as the content of polyethylene was increased. The 10% blend of Chronoflex and UHMWPE produced samples with consistent appearance as the extrusion difficulty didn't seem to affect the print performance, which was observed on the 15% blends. In addition, it has been found that the addition of 10% wt. of UHMWPE into PCU may improve the wear resistance of the matrix, as well as that performance can be significantly reduced by increasing the concentration of UHMWPE to 20% wt. [98].

For these tests, the samples and the balls were observed with the laser scanning microscope, but little to no wear was detected. The surfaces of the samples showed negligible wear deformation considering the natural roughness and waviness of the 3D printed surfaces. Another positive result was that the counterface, the silicon nitride balls, showed clear formation of fluid film. Figure 4.3 pictures two of the balls, imaged with the LSCM right after testing.

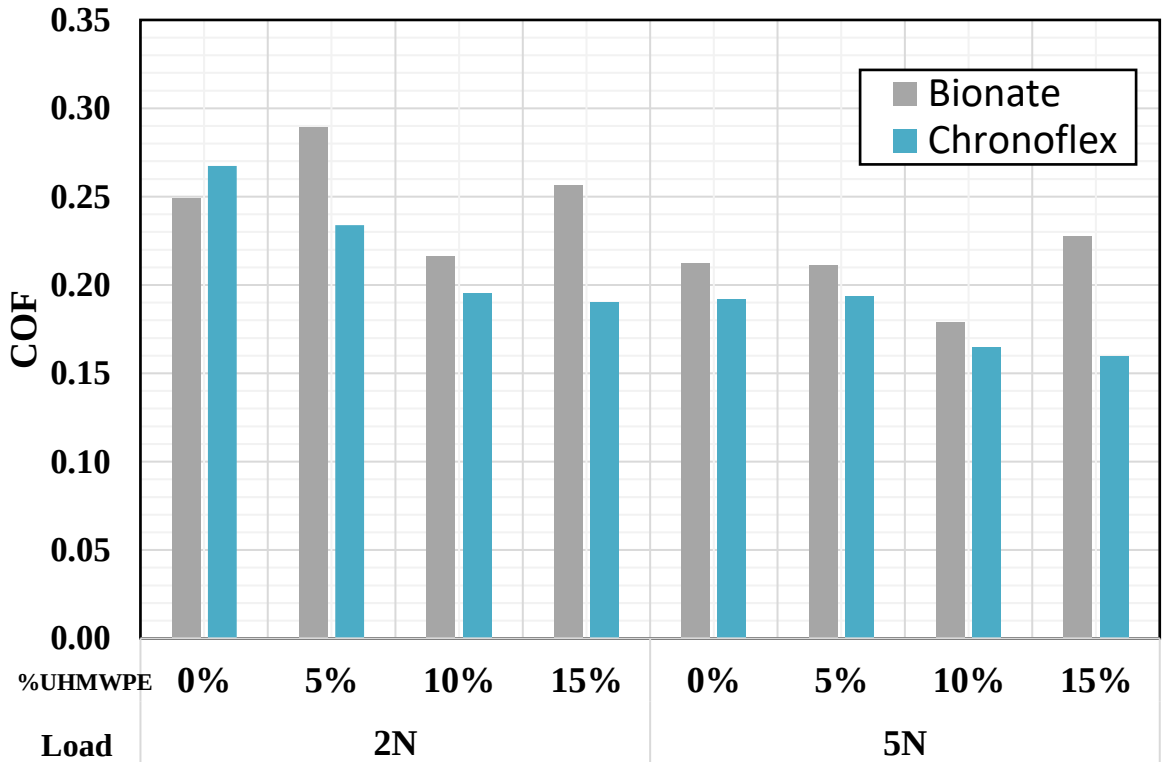

Fig. 4.2. Average COF of 3D printed Bionate and Chronoflex in the preliminary study.

It has been stated by literature that fluid film lubrication is part of the natural lubrication mechanisms of synovial joints [108,109]. Furthermore, it has been shown that silicon nitride balls tend to promote fluid film lubrication on polyethylene surfaces and carry a recurrent transition from fluid-film lubrication to boundary lubrication [110]. Although these results are encouraging, the lack of wear marks may be attributed to the short duration of the tests. Therefore, for the following friction tests, it was decided to run the tests for 8 hours, and well as to apply heavier loads to push the materials closer to their limits, accelerating the occurrence of wear mechanisms.

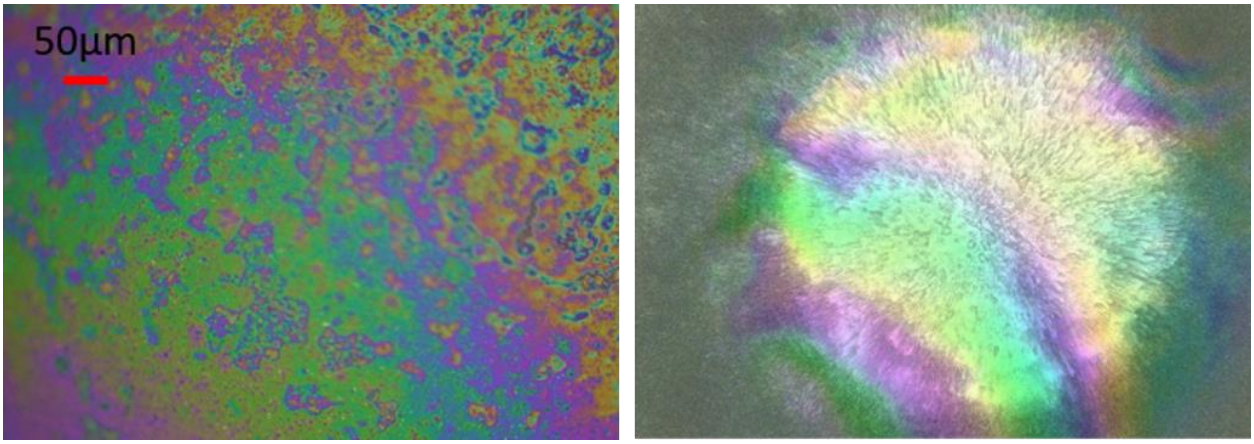

Fig. 4.3. Surface of silicon nitride ball imaged immediately after friction test shows formation of lubricant film.

4.2. In-depth study: Chronoflex and UHMWPE

Here are described the results related to the more comprehensive study of Chronoflex and UHMWPE, including molded and 3D printed parts.

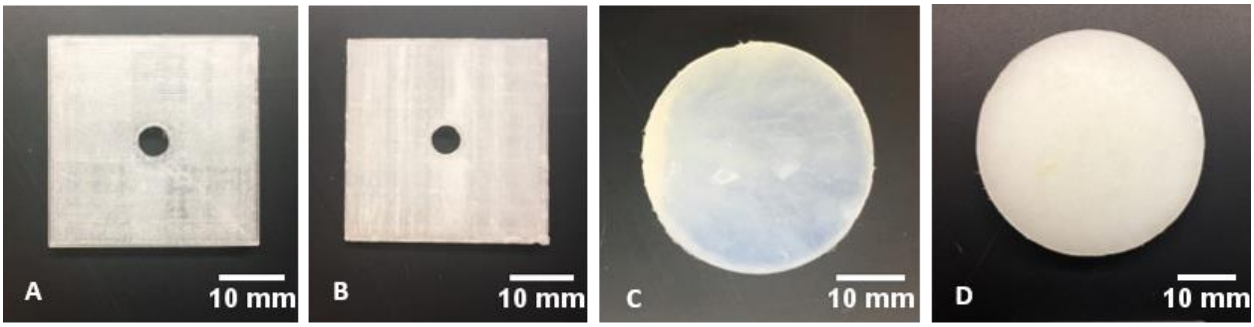

Fig. 4.4. Photos of the fabricated samples: (A) CF0, (B) CF10, (C) CFm, and (D) UHMWPEm.

4.2.1. Surface characterization

Laser scanning microscopy of the sample surfaces

Sample surfaces utilized for the friction tests can be seen on Fig. 4.4. Measurements taken with the laser scanning microscope, average surface roughness (S_a) and root mean square roughness (S_q), are summarized in Table 4. The microscope images of CF0 and CF10 show directional lines and voids, features that are inherent to 3D printing. Due to the molded surfaces

not have been polished, some marks are also observed on the molded samples, CFm and UHMWPEm. Despite the defects, molded samples still presented a lower surface roughness.

The blended 3D printed sample (CF10) showed the highest roughness (2.5 ± 0.4 µm), while the molded UHMWPE had the lowest roughness (1.1 ± 0.1 µm). The blended polymers were found to be not trivial to get filament fabricated and samples 3D printed, as compared to using only PCU. Occasional speed reductions and slightly inconsistent flow rates were observed during extrusion of CF10. Those may have resulted in higher roughness, which is, however, within the range of natural cartilage (2-5 µm) [111]. Besides, and most importantly, molded and 3D printed PCU showed comparable and lower surface roughness (CF0 1.5 ± 0.1 µm, and CFm 1.4 ± 0.1 µm).

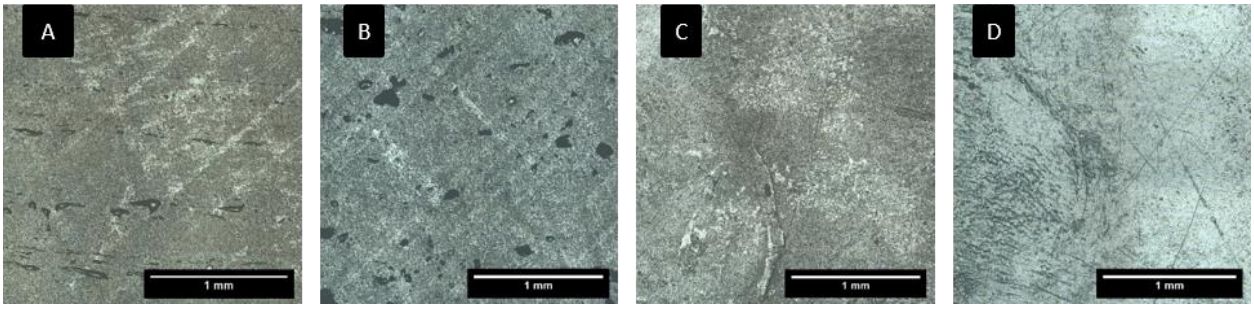

Fig. 4.5. Images of surfaces used for friction tests captured with laser scanning microscope. (A) CF0, (B) CF10, (C) CFm, and (D) UHMWPEm.

Table 4.1. Sample surface roughness.

Roughness	CF0	CF10	CFm	UHMWPEm
S_a (µm)	1.5 ± 0.1	2.5 ± 0.4	1.4 ± 0.1	1.1 ± 0.1
S_q (µm)	2.2 ± 0.3	4.1 ± 0.4	1.8 ± 0.1	2.1 ± 0.4

Water contact angle

Figure 4.5 shows that WCA of all four types of samples. No significant difference was found between the WCA of the samples. Furthermore, all the samples demonstrate a behavior with average WCAs less than 90°.

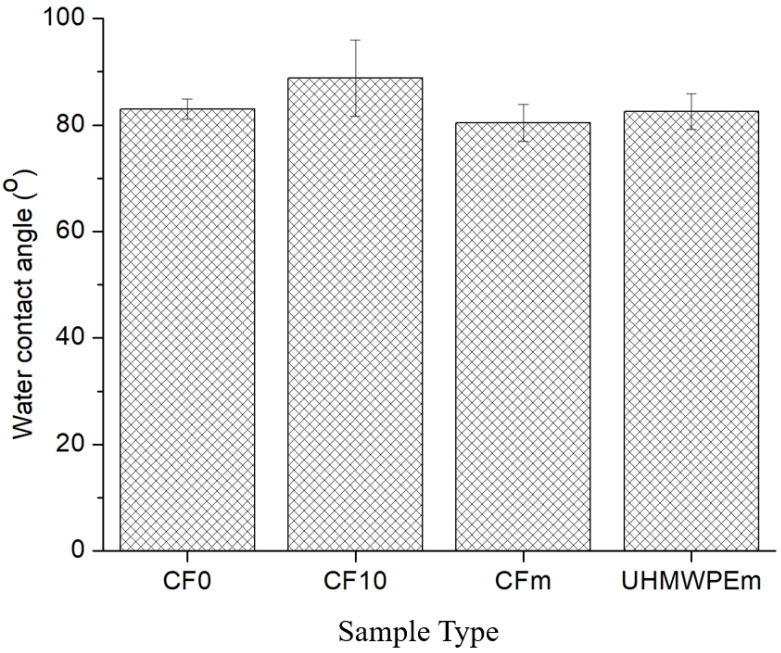

Fig. 4.6. Water contact angles of samples are found to be nearly the same.

4.2.2. Material characterization

Morphology of the sample internal structures

Samples prepared using microtome cut revealed diverse cross-sectional morphologies among the samples. SEM images in Fig. 4.6 show porosities on the 3D printed samples (Fig. 4.6 A and B) and micro/nano-scale roughness was found inside CF10 pores (Fig. 4.6 F). The micro/nano-sized structures that were observed inside some of those pores, are believed to be UHMWPE lamellae agglomerations that did not mix well to the PCU matrix.

It can be seen a higher concentration of pores on the CF10 sample surface (Fig. 4.6 B and F). Additionally, the pores on CF10 looked larger than the ones seen on CF0 cross-sectional area, vide Fig. 4.6 A and E. In short, 13.61% of CF10 cross-sectional area represented pores, while 6.34% of CF0 was pores. No pore features are seen on the cross-sectional surfaces of molded PCU. On the other hand, molded UHMWPE cross-sectional area present scars from the microtome cut (Fig. 4.6 D). Figure 4.6 H represents a higher magnification image of the UHMWPE cross-sectional surface, showing its microstructure, with non-spherical, entangled lamellae, typical of UHMWPE morphology [99,100,112].

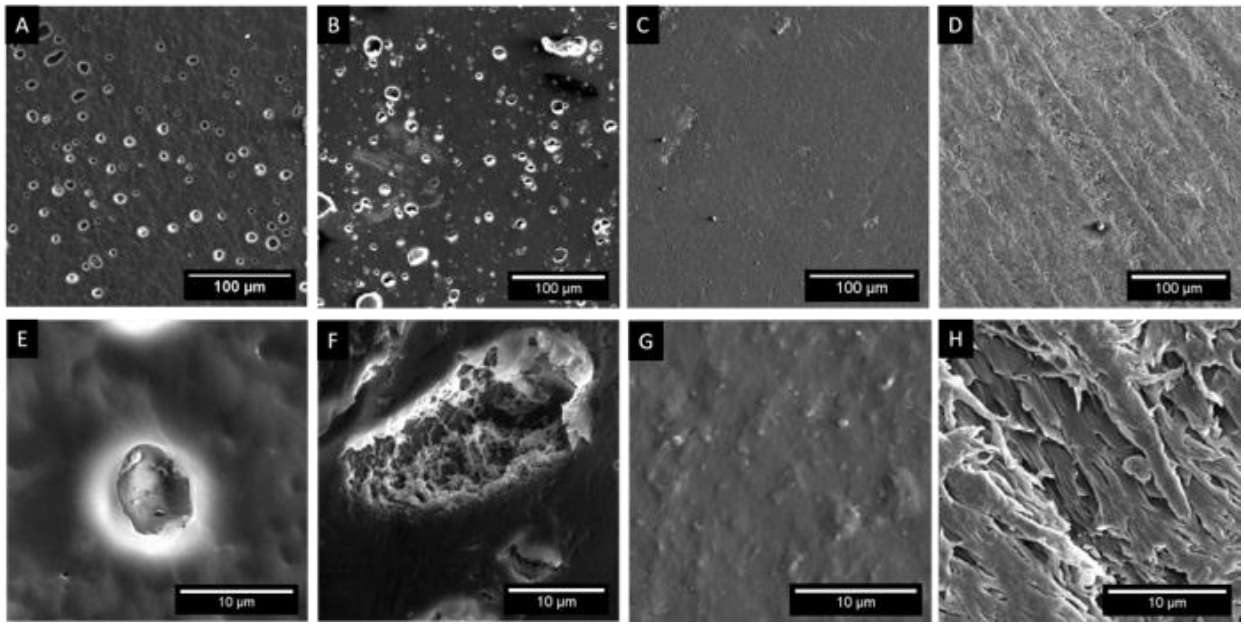

Fig. 4.7. SEM images of the cross-sectional areas of the samples cut through microtome technique. A through D represent CF0, CF10, CFm and UHMWPEm, respectively. Images E through H follow the same order and show higher magnification images.

XRD

The XRD spectra of all types of samples are reproduced on fig. 4.7. Polycarbonate-based thermoplastic urethanes have been found to have amorphous and partially crystalline structures [113]. From Fig. 4.7, we see that regardless the manufacturing method, the crystalline structures of PCU (CF0, CF10 and CFm) are consistent. It can also be seen that UHMWPE was

effectively added in CF10. The molded UHMWPE presented two peaks, around 2θ = 21.5° and 24°, which agree with literature reporting UHMWPE crystalline diffraction peaks at the mentioned angles [1].

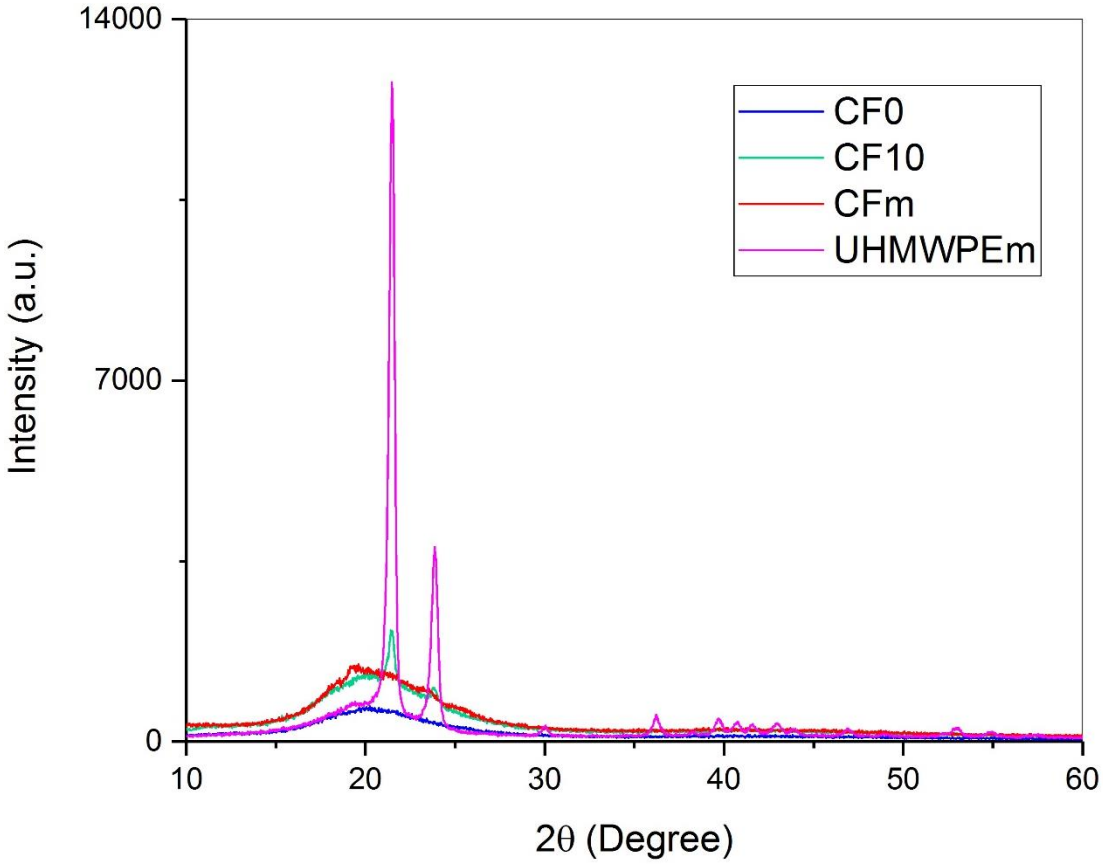

Fig. 4.8. XRD spectrum of composite sample (CF10) show the influence of adding UHMWPE in PCU with characteristic peaks from the crystallinity pattern of UHMWPE.

Absorption test

For the absorption tests, the samples were immersed in a solution of 30 vol. % bovine serum in water for durations ranging from 10 min to 24 hours. Figure 4.8 shows the absorption properties of all four types of samples. Different absorption capabilities were found among them, with that of the CF10 sample being the highest. The results are better comprehended considering the natural porosity of the 3D printed samples, they played an important role here. By depositing

the material layer by layer, and line-by-line, the FDM 3D printing fabrication method does not produce samples with a solid structure, although the printer was configured to deliver a 100% infill. This resulted in inherent micro-sized voids within the samples, which contributed to the increase of the capacity of fluid absorption of the already hydrophilic samples. As can be seen from Fig. 4.6, CF10 has the largest amount of porosity and the micro/nano-scale structures on the walls of the pores are believed to further enhance the sample's absorption properties. Figure 4.8 A shows the weight continues to increase over time for all PCU samples while the weight of UHMWPEm stabilized after the first 4 hours of immersion. We can also observe the curve representing CFm has a lower increasing trend compared to the 3D printed PCU samples.

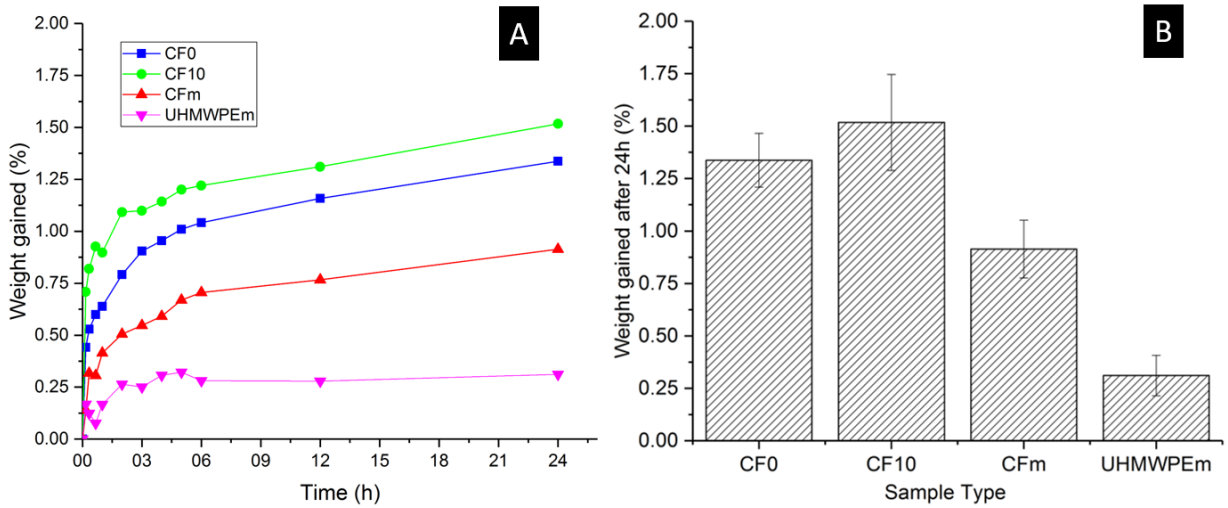

Fig. 4.9. (A) Absorption tests results present increasing weight over 24-hours immersion in bovine serum. (B) Average weight gain after total immersion time shows increasing trend with increasing amount of porosity. 3D printed samples present overall higher absorption rates.

In terms of the average weight gained after the 24-hour absorption period, Fig. 4.8 B, molded PCU (CFm) had an increment of about 0.9% from its original weight, which is in line with the value reported by the manufacturer (approximately 1%). Moreover, the 3D printed PCU samples resulted in up to 46.3% higher weight gain compared to the molded version of the same material (CF0).

4.2.3. Tribological testing and post-analysis

Figure 4.9 A shows the sample COF change over the test duration. The COF of the 3D printed samples are similar (Fig. 4.9 A), both presenting a decreasing trend after the first 15,000 seconds. The COF of molded PCU also tends to decrease but that behavior is observed throughout the entire test. UHMWPEm, however, yields a COF that stabilizes around halfway of testing. This trend differentiates from those of the PCU samples by having an increasing trend just before stabilizing.

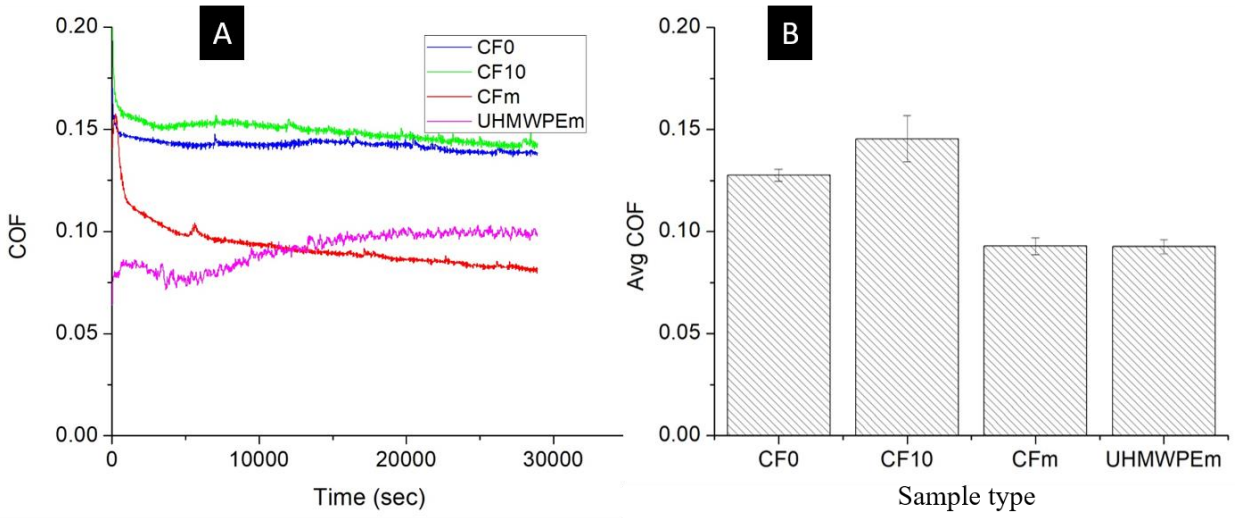

Fig. 4.10. COF of all four types of samples. (A) COF as a function of test duration. 3D printed samples showed higher COF but more steady curves. COF of CFm shows a decreasing trend. (B) Average COF for all samples. 3D printed samples showed higher COF than the molded samples.

Figure 4.9 B shows the average COF of the samples. CF10 showed a slightly higher COF than CF0, which may be explained by the lower printing quality of the samples with the addition of UHMWPE, and consequently higher S_a and S_q, as shown in Table 4. Overall, the 3D printed samples generated a higher surface roughness which resulted in a greater average COF than the molded samples. Nevertheless, the COF profiles were stable over time and within the range cited by other published literature [3].

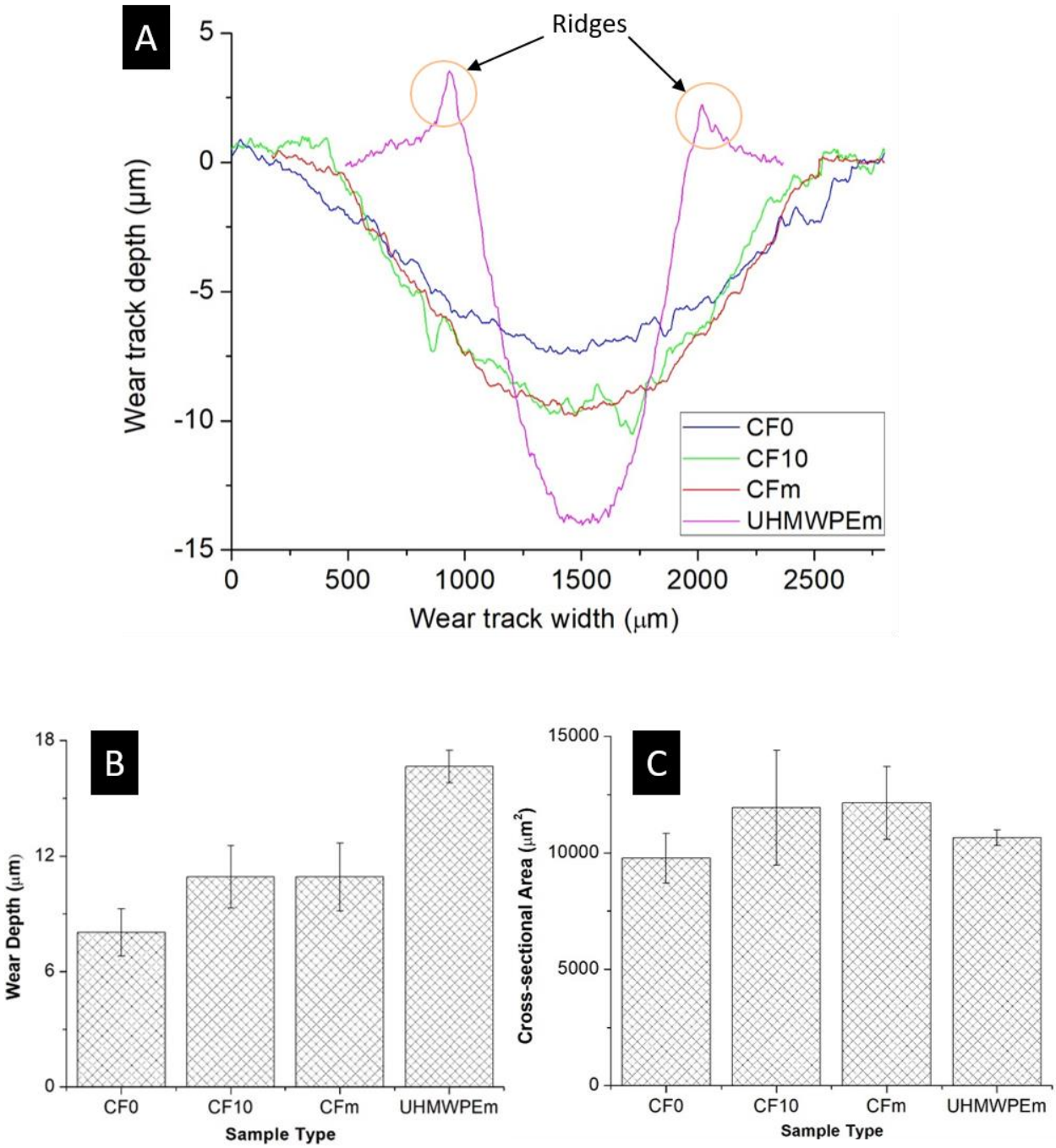

Fig. 4.11. (A) Average wear track profiles show the disparities between molded UHMWPE and PCU samples. The wear depths of CF0 is much smaller than that of UHMWPEm wear track (B), even though cross-sectional areas are similar (C).

The wear track was quantified with Keyence Multi-File Analyzer software, by comparing the wear track profiles, their depth, and cross-sectional area, as shown in Fig. 4.10. The deepest profile was found to be from the molded UHMWPE, and the shallowest, from the 3D

printed PCU (CF0). All samples have similar wear track appearance, as seen on Fig. 4.11. Their wear track profiles also have analogous shape, with same width, but different depths, vide Fig. 4.10. In addition to the deepest wear track profile, UHMWPEm also produced sharp edges on the surface at the ridges of the wear tracks, common to plastic deformation, pitting and fatigue wear [114–116]. Those sharp ridges (Fig. 4.10 A) may cause local stress concentration, which could lead to further plastic deformation and ultimately cause detachment of UHMWPE particles due to fatigue wear.

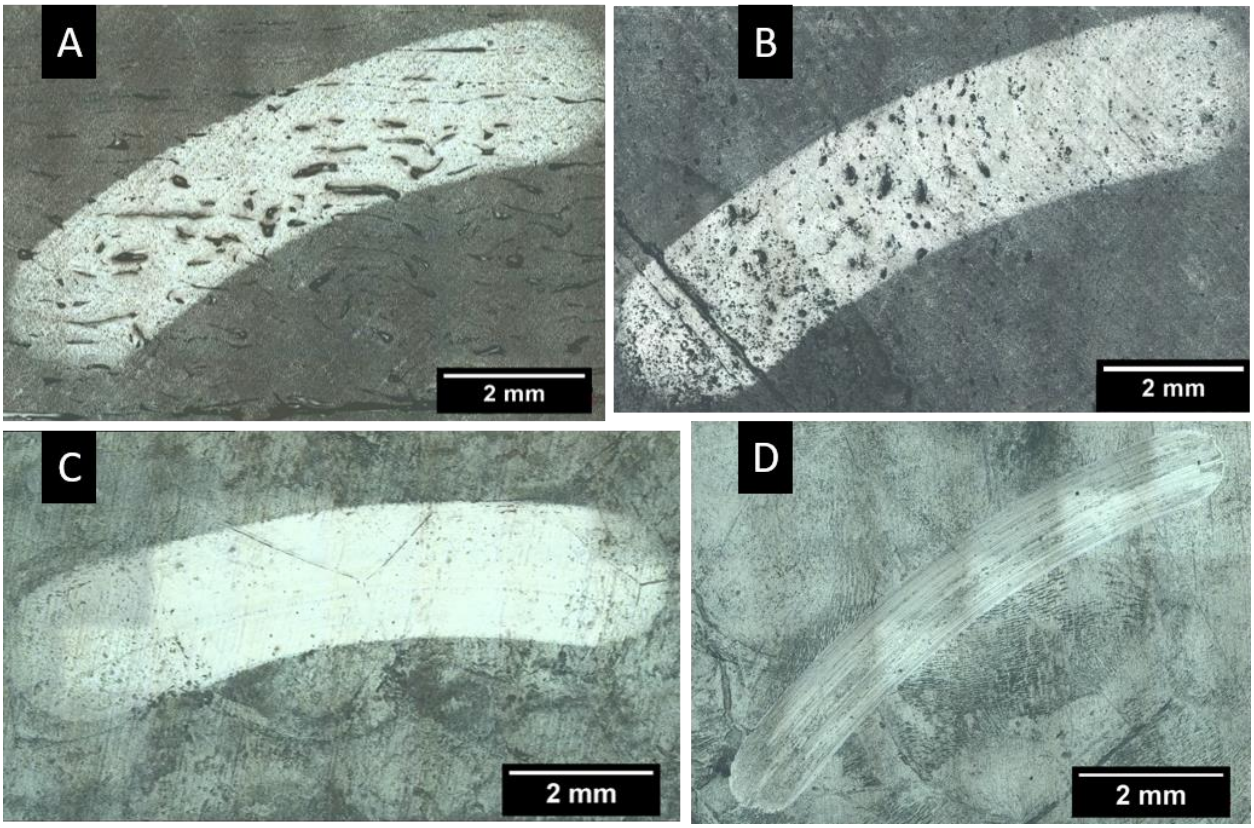

Fig. 4.12. Optical images of the wear tracks from laser scanning microscope. (A) CF0, (B) CF10, (C) CFm, and (D) UHMWPEm.

Published works have shown that PCU not only yields a lower wear rate compared to UHMWPE, but also, in general, generates wear particles that are larger in size, and that are relatively less harmful to the joint [8,117]. Although phagocytosis of wear debris is size dependent,

a high concentration of submicron-sized particles induces significant level of secretion of bone resorbing factors [118]. Since the printed PCU (CF0) had a lower cross-section area of wear track than the molded PCU, the volume of the wear debris would be reduced as well. Hence, possible risks of adverse biological responses from the wear debris of CF0 is expected to be less compared to that of molded PCU.

Contrary to what was expected, CF10 did not yield an improved wear performance. A study demonstrated lower wear rate by adding 10% wt. of UHMWPE powder in a thermoplastic polyurethane matrix [22]. However, the blend was fabricated via compression molding, while our method was FDM 3D printing. The crystallinity of the polymers was found to remain unaffected by the fabrication processes we adopted. The XRD profiles showed no significant difference between molded and 3D printed samples (Fig. 4.7). Yet, the high porosity area ratio may have impacted mechanical strength and resulted in a higher wear rate than that of CF0 [119].

In summary, the fabrication method has proven to be of considerable importance: 3D printed PCU samples resulted in 27% lower wear-track depth compared to molded PCU samples ($p < 0.05$). That is believed to be enabled by the enhanced lubrication behavior through the porosity of the 3D printed samples. As in natural menisci, the porous structure absorbs and releases synovial fluid with an applied load and maintaining the separation between the opposite rubbing surfaces. A recent study, conducted by Miller at al., evidenced that 3D printed PCU matched or outperformed the results of molded PCU in terms of monotonic mechanical testing, shear and fatigue tests [120]. Therefore, we could say that 3D printed PCU are wear resistant, mechanically strong and have the capability of providing menisci-like lubricant mechanism.

Chapter 5

CONCLUSIONS

This study explored the potential of using FDM 3D printing for fabricating compliant biocompatible materials for artificial meniscus implant. Compression molded PCU and UHMWPE were fabricated to compare to the 3D printed pure PCU and 10 wt.% PCU/UHMWPE blend. It was found that it is feasible to fabricate 3D printed PCU/UHMWPE blend. However, even though 3D printed blend benefited from its multiscale porous structure, it had similar wear to the molded PCU due to a higher surface roughness. On the other hand, 3D printed PCU showed a significant wear reduction through maintaining its flexibility and benefiting from its porous structure. Therefore, it can be concluded that the FDM additive manufacturing method may be a good alternative to the fabrication of PCU meniscus implants as it generated the lowest wear depth and was able to increase bovine serum solution absorption compared to the molded version of the same material.

This study explored the potential of FDM 3D printing as a fabrication method of porous, compliant artificial meniscus implant, particularly using PCU as a matrix. The main goal was to benefit from the freedom of design of this additive manufacturing method in order to introduce porosity in the structure of a flexible biocompatible polymer or polymeric blend, to be used in artificial meniscus implants. By having a porous architecture, meniscus implants will enable synovial fluid to lubricate the joint through “weeping” lubrication, a natural mechanism of the synovial joints that only happens because of the inherent porosity of the cartilage. The success of joints’ implants depends not only on the mechanical properties of the chosen material for the replacement, but also on their interaction with the in vivo environment, which includes the way they will promote the joint’s lubrication. There have been great efforts towards finding a suitable

soft material that resembles human synovial joint cartilage in terms of mechanical properties, long-term biocompatibility, and wear resistance. Current alternatives for meniscus injuries treatment involve different kinds of non-invasive therapies, as well as surgical approaches, such as acquiring a meniscus allograft or inserting a bio-resorbable implant. However, each option carries extra complications and none of them is a permanent solution. NUsurface® is the first permanent meniscus implant in the market. It is made of an excellent combination of materials, but its molded solid structure may compromise the long- term performance of the implant because it hinders synovial joints' natural lubrication mechanisms due to the lack of porosity in its structures.

The first step of this research was to develop a process with a set of parameters that produced samples with consistent quality for the friction tests. Much of this procedure was done with Ninjaflex, and that way temperatures, print speeds, distances and flow rates, for example, were adjusted initially with that thermoplastic urethane, and later transferred to polycarbonate urethane. A first set of friction tests was performed with Ninjaflex, evaluating how the orientation of the samples could affect their tribological properties. By rotating the sample 45° relative to the print bed, the print pattern was still the same but oriented differently because the sample sides had moved. They were then tested on a rotational oscillating friction tester under water for 30 minutes. Even though the testing time was short, it was possible to identify that printing with rectilinear pattern parallel to the sides (90°) of the sample can result in COF curves that yield to stability faster than the other orientation. From that point on, all 3D printed samples were printed using the same architecture orientation.

A second set of preliminary tests was done comparing Bionate and Chronoflex as PCU alternatives for this project. UHMWPE was used to blend with each type of PCU at 5, 10 and 15% weight concentrations and evaluate how they function during the fabrication process and whether

the results of 2-hour friction tests would have any difference between them. It was found that it is feasible to fabricate 3D printed PCU/UHMWPE blends despite their very different melt flow indexes. For each of the mentioned loads and UHMWPE concentration, Bionate presented a higher COF compared to Chronoflex under the same testing conditions, in most of the tests. Samples and balls were observed after testing on the LSCM: any of the 3D printed samples exhibited considerable wear, and the surfaces of the balls seemed to produce a layer of lubricant fluid film. Those results were considered promising, since the formation of fluid film is one of the characteristics of the natural knee joint lubrication. However, we did not observe significant wear on PCU samples, which may be explained by the short duration of the tests of the light load applied, although the calculated contact pressure was within the stress range carried by the meniscus cartilage. Thus, for a more comprehensive testing series, it was decided to increase the load and the testing duration.

The in-depth study was conducted only using Chronoflex as PCU, since the results of the preliminary tests showed that polymer had a lower COF. 10% weight concentration of UHMWPE was the only one studied because of its good results from the extrusion processes. Compression molded PCU and UHMWPE were fabricated to compare to the 3D printed pure PCU and 10 wt.% PCU/UHMWPE blend. Results showed that, even though 3D printed blend benefited from its multiscale porous structure, it had similar wear to the molded PCU due to a higher surface roughness. On the other hand, 3D printed pure PCU showed a significant wear reduction through maintaining its flexibility and benefiting from its porous structure. Although the amount of porosity increased and fluid absorption capability was enhanced for the CF10 samples, the average wear resistance may be an indication that there should be a balance on the extent of porosity. In other words, there may be a compromise between inserting more porous structures and keeping a

sturdy bulk that withstands tribological and mechanical demands. Therefore, it can be concluded that the FDM additive manufacturing method may be a good alternative to the fabrication of PCU meniscus implants as it generated the lowest wear depth and was able to increase bovine serum solution absorption compared to the molded version of the same material.

FUTURE DIRECTIONS

This research has found that it is possible to 3D print blends of PCU/UHMWPE using FDM technology. That was accomplished by using a print head made to print flexible materials, which constraints the filament path to the nozzle. Although the Lulzbot TAZ 6 is an excellent machine for its kind, desktop FDM 3D printer, it was not designed targeting the production of prints for biomedical applications. It is expected that by controlling the environment where the sample is fabricated, there could be less contamination and therefore lower risks during the application. Furthermore, an investigation with different diameters of extrusion nozzles could improve the results by tailoring the printed structure porosity and achieving better control of print parameters. It is possible that the surface of the samples could become smoother if that control is increased. Achieving a smoother surface throughout the entire 3D printed sample is ideal, while herein the surface in contact with the print bed was used to avoid the high roughness of the top surface. A polishing step could be added after printing, but that goes against the proposed practicality and convenience of using the complexity-free FDM 3D printing fabrication method.

A future endeavor for this research is to be able to 3D print a meniscus from a magnetic resonance imaging (MRI) scan. The unique curved surfaces of the natural meniscus make it challenging for it to be 3D printed, but not impossible. There should be a study on how support structures could be included in the print design in order to hold the meniscus the best way possible. Again, the resulting surface quality will be another concern, since the layer-by-layer pattern leaves an evident waviness, especially on curved lateral surfaces. A testing apparatus that is able to accommodate the meniscus shape would also be necessary to thoroughly evaluate it under in vitro conditions. Some researchers have built their own apparatus to test joint implant material, but adopting a simplified shape and neglecting the shape of the actual implant [62,74]. To further

assess the performance of the implants, other measurements could be done while running friction tests: wear particle measurements (quantify the number of particles released in the lubricant, measure their sizes and evaluate their shapes) and real contact area measurement through image and/or pressure sensing (to analyze pressure distribution). Tests that last millions of cycles would also help evaluate the use of the implant at a long-term perspective.

Finally, it is important to evaluate the mechanical properties of the 3D printed parts and compare to molded parts. Monotonic and tensile fatigue testing have been performed on 3D printed Bionate [94], but the compression efforts are dominant on the meniscus. An adaptation of a universal mechanical tester is usually the approach, such as the experimental validation done by Elsner et al. to validate a finite element analysis of the NUsurface® is a good example of in vitro mechanical test [33,121,122].

REFERENCES

[1] M. Hilal Maradit-Kremers, MD, MSc, Rochester, M. Cynthia S. Crowson, Rochester, M. Dirk Larson, Rochester, V. William A. Jiranek, MD, Richmond, M. Daniel J. Berry, MD, Rochester, Prevalence of Total Hip (THA) and Total Knee (TKA) Arthroplasty in the United States, 2014. https://www.mayoclinic.org/medical-professionals/clinical-updates/orthopedic-surgery/study-hip-knee-arthroplasty-shows-7-2-million-americans-living-with-implants.

[2] A.C.T. Vrancken, P. Buma, T.G. van Tienen, Synthetic meniscus replacement: a review, Int. Orthop. 37 (2013) 291–299. doi:10.1007/s00264-012-1682-7.

[3] S.E. Majd, A.I. Rizqy, H.J. Kaper, T.A. Schmidt, R. Kuijer, An in vitro study of cartilage-meniscus tribology to understand the changes caused by a meniscus implant, Colloids Surfaces B Biointerfaces. 155 (2016) 51–71. doi:10.1016/j.colsurfb.2017.04.034.

[4] I.D. McDermott, A.A. Amis, The consequences of meniscectomy, J. Bone Jt. Surg. - Br. Vol. 88–B (2006) 1549–1556. doi:10.1302/0301-620X.88B12.18140.

[5] P.R. Allen, R. a Denham, a V Swan, Late degenerative changes after meniscectomy. Factors affecting the knee after operation., J. Bone Joint Surg. Br. 66 (1984) 666–671.

[6] E. Balint, C.J. Gatt, M.G. Dunn, Design and mechanical evaluation of a novel fiber-reinforced scaffold for meniscus replacement, J. Biomed. Mater. Res. - Part A. 100 A (2012) 195–202. doi:10.1002/jbm.a.33260.

[7] J.J. Elsner, S. Portnoy, G. Zur, F. Guilak, A. Shterling, E. Linder-Ganz, Design of a Free-Floating Polycarbonate-Urethane Meniscal Implant Using Finite Element Modeling and Experimental Validation, J. Biomech. Eng. 132 (2010) 95001. doi:10.1115/1.4001892.

[8] J.J. Elsner, Y. Mezape, K. Hakshur, M. Shemesh, E. Linder-Ganz, A. Shterling, N. Eliaz, Wear rate evaluation of a novel polycarbonate-urethane cushion form bearing for artificial hip joints, Acta Biomater. 6 (2010) 4698–4707. doi:10.1016/j.actbio.2010.07.011.

[9] A. Burger, Feasibility Assessment of Compliant Polymers in TKR, (2009).

[10] S.E. Majd, R. Kuijer, T.A. Schmidt, P.K. Sharma, Role of hydrophobicity on the adsorption of synovial fluid proteins and biolubrication of polycarbonate urethanes: Materials for permanent meniscus implants, Mater. Des. 83 (2015) 514–521. doi:10.1016/j.matdes.2015.06.075.

[11] J. Charnley, The lubrication of animal joints in relation to surgical reconstruction by arthroplasty, Ann. Rheum. Dis. 19 (1960) 10–19. doi:10.1136/ard.19.1.10.

[12] J.B. Morrison, The mechanics of the knee joint in relation to normal walking, J. Biomech. 3 (1970) 51–61. doi:10.1016/0021-9290(70)90050-3.

[13] G. Kolata, Why “useless” surgery is still popular?, Upshot, New York Times. (2016). https://www.nytimes.com/2016/08/04/upshot/the-right-to-know-that-an-operation-is-next-to-useless.html (accessed August 30, 2017).

[14] Arthroscopic Surgery for Meniscal Tears May Be Unnecessary in Many Cases, (n.d.). http://www.moveforwardpt.com/didyouknow/detail.aspx?cid=d25686d3-b0e5-4ad3-b886-da74452dddb2.

[15] Meniscus Tears, (2014). http://orthoinfo.aaos.org/topic.cfm?topic=a00358 (accessed August 31, 2017).

[16] C. Baynat, C. Andro, J.P. Vincent, P. Schiele, P. Buisson, F. Dubrana, F.X. Gunepin, Actifit synthetic meniscal substitute: Experience with 18 patients in Brest, France, Orthop. Traumatol. Surg. Res. 100 (2014) S385–S389. doi:10.1016/j.otsr.2014.09.007.

[17] M. Majewski, H. Susanne, S. Klaus, Epidemiology of athletic knee injuries: A 10-year study, Knee. 13 (2006) 184–188. doi:10.1016/j.knee.2006.01.005.

[18] J.J. Elsner, B.P. Mckeon, Orthopedic Application of Polycarbonate Urethanes: A Review, in: 2017: pp. 1–9.

[19] M. KL, A. AM, Essential Clinical Anatomy (copy 2), Fifth, LWW, 2002.

[20] W.H. Brenno Nigg, Biomechanics of the Musculo-sketelal System, Third Edit, Wiley, 2007.

[21] A. Carré, V. Lacarrière, How Substrate Properties Control Cell Adhesion. A Physical–Chemical Approach, J. Adhes. Sci. Technol. 24 (2010) 815–830. doi:10.1163/016942409X12598231567862.

[22] D.D. Bernard J. Hamrock, Ball bearing lubrication: the elastohydrodynamics of elliptical contacts, NASA Technical Reports, Cleveland, Ohio, 1981.

[23] B.J. Hamrock, Fundamentals of Fluid Film Lubrication, NASA Reference Publication, Columbus, Ohio, 1991.

[24] A. Unsworth, Recent developments in the tribology of artificial joints, Tribol. Int. 28 (1995) 485–495. doi:10.1016/0301-679X(95)00027-2.

[25] D. Dowson, J.Q. Yao, Elastohydrodynamic lubrication of soft-layered solids at elliptical contacts: Part 2: film thickness analysis, Arch. Proc. Inst. Mech. Eng. Part J J. Eng. Tribol. 1994-1996 (Vols 208-210). 208 (2006) 43–52. doi:10.1243/PIME_PROC_1994_208_348_02.

[26] J. Klein, Molecular mechanisms of synovial joint lubrication, Proc. Inst. Mech. Eng. Part J J. Eng. Tribol. 220 (2006) 691–710. doi:10.1243/13506501JET143.

[27] J.H. Dumbleton, The Lubrication of Natural Joints, in: J.H.B.T.-T.S. Dumbleton (Ed.), Tribol. Nat. Artif. Joints, 1st editio, Elsevier, 1981: p. 479. doi:https://doi.org/10.1016/S0167-8922(08)71011-3.

[28] U.P. Hemmerich, A.; Brown, H.; Smith, S.; Marthandam, S.S.K.; Wyss, Hip, knee, and ankle kinematics of high range of motion activities of daily living., J. Orthop. Res. (2006) 770–781. doi:10.1002/jor.

[29] J. Rose, J.G. Gamble, Human Walking, Lippincott Williams & Wilkins, 2006. https://books.google.com/books?id=q6WrPwAACAAJ.

[30] A.E. Yousif, A.M. Ali, The Role of Lubrication Mechanisms in the Knee Synovial Joints, 1 St Reg. Conf. Eng. Sci. NUCEJ Spat. ISSUE. 1111 (2008) 522–535. http://www.iasj.net/iasj?func=fulltext&aId=29817%0Ahttp://www.iasj.net/iasj?func=search&template=&uiLanguage=en&query=The+Role+of+Lubrication+Mechanisms+in+the+Knee+Synovial+Joints&x=0&y=0.

[31] C.W. McCUTCHEN, Mechanism of animal joints: Sponge-hydrostaic and weeping

bearings, Nature. 184 (1959) 1284–1285. doi:10.1038/183055a0.

[32] P.K. Levangie, C.C. Norkin, Joint Structure and Function: A Comprehensive Analysis, F.A. Davis Company, 2005. https://books.google.com/books?id=DW9vQgAACAAJ.

[33] T. Fukubayashi, H. Kurosawa, THE CONTACT AREA AND PRESSURE DISTRIBUTION PATTERN OF THE KNEE A Study of Normal and Osteoarthrotic Knee Joints, Acta Orthop. Wand. 51 (1980) 871–879. http://www.tandfonline.com/doi/pdf/10.3109/17453678008990887 (accessed March 21, 2017).

[34] D.C. Fithian, M.A. Kelly, V.C. Mow, Material properties and structure-function relationships in the menisci., Clin. Orthop. Relat. Res. (1990) 19–31.

[35] S.R. Oungoulian, Friction and Wear Measurments of Bovine Articular Cartilage Against Non - Native Materials, Columbia University, 2015.

[36] W.R. Taylor, M.O. Heller, G. Bergmann, G.N. Duda, Tibio-femoral loading during human gait and stair-climbing, J. Orthop. Res. 22 (2004) 625–632. doi:10.1016/j.orthres.2003.09.003.

[37] S.L. Smith, H.E. Ash, A. Unsworth, A tribological study of UHMWPE acetabular cups and polyurethane compliant layer acetabular cups, J. Biomed. Mater. Res. 53 (2000) 710–716. doi:10.1002/1097-4636(2000)53:6<710::AID-JBM14>3.0.CO;2-R.

[38] A. Unsworth, Tribology of Human and Artificial Joints, Proc. Inst. Mech. Eng. Part H J. Eng. Med. 205 (1991) 163–172. doi:10.1243/PIME_PROC_1991_205_287_02.

[39] D.B. Chaffin, G. Andersson, Occupational Biomechanics, Wiley, 1991. https://books.google.com/books?id=3PFqAAAAMAAJ.

[40] D. Dowson, Z.M. Jin, Micro-elastohydrodynamic lubrication of synovial joints, Eng Med. 15 (1986) 63–65. doi:10.1243/EMED.

[41] D. Dowson, Elastohydrodynamic and micro-elastohydrodynamic lubrication, Wear. 190 (1995) 125–138. doi:10.1016/0043-1648(95)06660-8.

[42] V. Mosnegutu, V. Chiroiu, R. Ioan, On the friction coefficient of synovial fluid in knee joint, in: SISOM 2009 Sess. Comm. Acoust., 2009: pp. 148–152.

[43] P.S. Walker, J. Sikorski, D. Dowson, M.D. Longfield, V. Wright, T. Buckley, Behaviour of synovial fluid on surfaces of articular cartilage. A scanning electron microscope study., Ann. Rheum. Dis. 28 (1969) 1–14. http://www.ncbi.nlm.nih.gov/pubmed/5786278%5Cnhttp://www.pubmedcentral.nih.gov/articlerender.fcgi?artid=PMC1010488.

[44] A.P. Harsha, T.J. Joyce, Challenges associated with using bovine serum in wear testing orthopaedic biopolymers, Proc. Inst. Mech. Eng. Part H J. Eng. Med. 225 (2011) 948–958. doi:10.1177/0954411911416047.

[45] T. Peters, All About Albumin: Biochemistry, Genetics, and Medical Applications. . San Diego, CA: Academic Press, 1996, 432 pp, $85.00. ISBN 0-12-552110-3, Clinical Chemistry, 1995. http://clinchem.aaccjnls.org/content/43/10/2014a.

[46] T.A. Schmidt, R.L. Sah, Effect of synovial fluid on boundary lubrication of articular cartilage, Osteoarthr. Cartil. 15 (2007) 35–47. doi:10.1016/j.joca.2006.06.005.

[47] A. Wang, A. Essner, G. Schmidig, The effects of lubricant composition on in vitro wear testing of polymeric acetabular components, J. Biomed. Mater. Res. B. Appl. Biomater. 68 (2004) 45–52. doi:10.1002/jbm.b.10077.

[48] M.E. Blewis, G.E. Nugent-Derfus, T.A. Schmidt, B.L. Schumacher, R.L. Sah, A model of synovial fluid lubricant composition in normal and injured joints, Eur. Cells Mater. 13 (2007) 26–38. doi:10.1186/ar3216.

[49] R. Trebše, A. Miheli, Joint Replacement: Historical Overview, in: Infected Total Jt. Arthroplast., 2012: pp. 7–11. doi:10.1007/978-1-4471-2482-5.

[50] D.H. Williams, D.S. Garbuz, Masri, Total knee arthroplasty; techniques and results, Bc Med. J. 52 (2010) 447–454.

[51] M.L. Wolford, K. Palso, A. Bercovitz, P.D. Monica L. Wolford, M.A.; Kathleen Palso, M.A.; and Anita Bercovitz, M.P.H., Hospitalization for Total Hip Replacement Among Inpatients Aged 45 and Over: United States, 2000–2010, 2015. doi:ISSN 1941–4935.

[52] J.M. Lee, F.H. Fu, The meniscus: basic science and clinical applications, Oper. Tech. Orthop. 10 (2000) 162–168. doi:10.1053/otor.2000.5289.

[53] A.M. Ahmed, D.L. Burke, In-Vitro of Measurement of Static Pressure Distribution in Synovial Joints—Part I: Tibial Surface of the Knee, J. Biomech. Eng. 105 (1983) 216–225. http://dx.doi.org/10.1115/1.3138409.

[54] M.E. Baratz, F.H. Fu, R. Mengato, Meniscal tears: The effect of meniscectomy and of repair on intraarticular contact areas and stress in the human knee: A preliminary report, Am. J. Sports Med. 14 (1986) 270–275. doi:10.1177/036354658601400405.

[55] E.A. Makris, P. Hadidi, K.A. Athanasiou, The knee meniscus: Structure–function, pathophysiology, current repair techniques, and prospects for regeneration, Biomaterials. 32 (2011) 7411–7431. doi:10.1016/j.biomaterials.2011.06.037.

[56] D.D. Lin, N.E. Picardo, A. Adesida, W.S. Khan, Clinical Studies Using Biological and Synthetic Materials for Meniscus Replacement., Curr. Stem Cell Res. Ther. (2016) 1–6. doi:10.2174/1574888X11666160429123.

[57] C. Van Der Straeten, P. Byttebier, A. Eeckhoudt, J. Victor, Meniscal Allograft Transplantation Does Not Prevent or Delay Progression of Knee Osteoarthritis, PLoS One. 11 (2016) e0156183. doi:10.1371/journal.pone.0156183.

[58] J.J. Rongen, T.G. van Tienen, B. van Bochove, D.W. Grijpma, P. Buma, Biomaterials in search of a meniscus substitute, Biomaterials. 35 (2014) 3527–3540. doi:10.1016/j.biomaterials.2014.01.017.

[59] N.A. Smith, M.L. Costa, T. Spalding, Instructional review: Knee Meniscal allograft transplantation: Rationale for treatment, Bone Jt. J. 97–B (2015) 590–594. doi:10.1302/0301-620X.97B5.35152.

[60] A.C.T. Vrancken, P. Buma, T.G. Van Tienen, Synthetic meniscus replacement: A review, Int. Orthop. 37 (2013) 291–299. doi:10.1007/s00264-012-1682-7.

[61] J. de Groot, Actifit, Polyurethane meniscus implant: basic science, in: The Meniscus, Springer Berlin Heidelberg, Berlin, Heidelberg, 2010: pp. 383–387. doi:10.1007/978-3-642-02450-4_48.

[62] A. Chyr, A.P. Sanders, B. Raeymaekers, A hybrid apparatus for friction and accelerated wear testing of total knee replacement bearing materials, Wear. 308 (2013) 54–60. doi:10.1016/j.wear.2013.09.017.

[63] A.J. Sophia Fox, A. Bedi, S.A. Rodeo, The Basic Science of Articular Cartilage, Sports Health. 1 (2009) 461–468. doi:10.1177/1941738109350438.

[64] A.M. Hukins D., The Extracellular Matrix of the Meniscus, Raven Press, New York, NY, 1992.

[65] G. Zur, E. Linder-ganz, J.J. Elsner, J. Shani, O. Brenner, G. Agar, E.B. Hershman, S.P. Arnoczky, F. Guilak, A. Shterling, Chondroprotective effects of a polycarbonate-urethane meniscal implant: histopathological results in a sheep model, Knee Surgery, Sport. Traumatol. Arthrosc. 19 (2011) 255–63. doi:http://0-dx.doi.org.library.uark.edu/10.1007/s00167-010-1210-5.

[66] E. Linder-Ganz, J.J. Elsner, A. Danino, F. Guilak, A. Shterling, A Novel Quantitative Approach for Evaluating Contact Mechanics of Meniscal Replacements, J. Biomech. Eng. 132 (2010) 24501. doi:10.1115/1.4000407.

[67] T. De Coninck, J.J. Elsner, E. Linder-Ganz, M. Cromheecke, M. Shemesh, W. Huysse, R. Verdonk, K. Verstraete, P. Verdonk, In-vivo evaluation of the kinematic behavior of an artificial medial meniscus implant: A pilot study using open-MRI, Clin. Biomech. 29 (2014) 898–905. doi:10.1016/j.clinbiomech.2014.07.001.

[68] T. Hügle, J. Geurts, C. Nüesch, M. Müller-Gerbl, V. Valderrabano, Aging and osteoarthritis: An inevitable encounter?, J. Aging Res. 2012 (2012). doi:10.1155/2012/950192.

[69] H.J. Bieleman, M.W. Van Ittersum, J.W. Groothoff, J.C.M. Oostveen, F.G.J. Oosterveld, C.P. Van Der Schans, R. Soer, M.F. Reneman, Functional capacity of people with early osteoarthritis: A comparison between subjects from the cohort hip and cohort knee (CHECK) and healthy ageing workers, Int. Arch. Occup. Environ. Health. 83 (2010) 913–921. doi:10.1007/s00420-010-0541-3.

[70] A.T. Miller, Fatigue and cyclic loading of 3D printed soft polymers for orthopedic applications, Georgia Institute of Technology, 2017.

[71] G. Chakrabarty, M. Vashishtha, D. Leeder, Polyethylene in knee arthroplasty: A review, J. Clin. Orthop. Trauma. 6 (2015) 108–112. doi:10.1016/j.jcot.2015.01.096.

[72] H. Oonishi, Y. Kadoya, S. Masuda, Gamma-irradiated cross-linked polyethylene in total hip replacements--analysis of retrieved sockets after long-term implantation., J. Biomed. Mater. Res. 58 (2001) 167–171.

[73] B. McEntire, B.S. Bal, A. Lakshminarayanan, R. Bock, Silicon Nitride Bearings for Total Joint Arthroplasty, Bone Jt. J. 98–B (2016) 34–34. http://www.bjjprocs.boneandjoint.org.uk/content/98-B/SUPP_1/34 (accessed January 26, 2017).

[74] C.J. Schwartz, S. Bahadur, Development and testing of a novel joint wear simulator and investigation of the viability of an elastomeric polyurethane for total-joint arthroplasty devices, Wear. 262 (2007) 331–339. doi:10.1016/j.wear.2006.05.018.

[75] T. Huang, S. Wang, K. He, Quality control for fused deposition modeling based additive

manufacturing: Current research and future trends, in: 2015: pp. 1–6. doi:10.1109/ICRSE.2015.7366500.

[76] H. Lipson, M. Kurman, Fabricated : The New World of 3D Printing (1), Wiley, Somerset, US, 2013. http://site.ebrary.com/lib/alltitles/docDetail.action?docID=10657814 (accessed April 12, 2016).

[77] A. Boschetto, L. Bottini, Design for manufacturing of surfaces to improve accuracy in Fused Deposition Modeling, Robot. Comput. Integr. Manuf. 37 (2016) 103–14. doi:10.1016/j.rcim.2015.07.005.

[78] O.A.M. Abdelaal, S.M.H. Darwish, Review of Rapid Prototyping Techniques for Tissue Engineering Scaffolds Fabrication, in: A. Öchsner, L.F.M. da Silva, H. Altenbach (Eds.), Springer Berlin Heidelberg, 2013: pp. 33–54. http://link.springer.com/chapter/10.1007/978-3-642-31470-4_3 (accessed April 15, 2016).

[79] T. Billiet, M. Vandenhaute, J. Schelfhout, S. Van Vlierberghe, P. Dubruel, A review of trends and limitations in hydrogel-rapid prototyping for tissue engineering, Biomaterials. 33 (2012) 6020–6041. doi:10.1016/j.biomaterials.2012.04.050.

[80] E.L. Melgoza, G. Vallicrosa, L. Serenó, J. Ciurana, C.A. Rodríguez, Rapid tooling using 3D printing system for manufacturing of customized tracheal stent, Rapid Prototyp. J. 20 (2014) 2–12. doi:10.1108/RPJ-01-2012-0003.

[81] D.H. Rosenzweig, E. Carelli, T. Steffen, P. Jarzem, L. Haglund, 3D-Printed ABS and PLA Scaffolds for Cartilage and Nucleus Pulposus Tissue Regeneration, Int. J. Mol. Sci. 16 (2015) 15118–15135. doi:10.3390/ijms160715118.

[82] A. Melocchi, F. Parietti, G. Loreti, A. Maroni, A. Gazzaniga, L. Zema, 3D printing by fused deposition modeling (FDM) of a swellable/erodible capsular device for oral pulsatile release of drugs, J. Drug Deliv. Sci. Technol. 30 (2015) 360–367. doi:https://doi.org/10.1016/j.jddst.2015.07.016.

[83] S.S. Crump, Apparatus and method for creating three-dimensional objects, n.d. http://www.google.com/patents/US5121329 (accessed April 11, 2016).

[84] M. Atif Yardimci, Selçuk Güçeri, Conceptual framework for the thermal process modelling of fused deposition, Rapid Prototyp. J. 2 (1996) 26–31. doi:10.1108/13552549610128206.

[85] M.H. Too, K.F. Leong, C.K. Chua, Z.H. Du, S.F. Yang, C.M. Cheah, S.L. Ho, Investigation of 3D Non-Random Porous Structures by Fused Deposition Modelling, Int. J. Adv. Manuf. Technol. 19 (2002) 217–223. doi:10.1007/s001700200016.

[86] Mukesh K. Agarwala, Vikram R. Jamalabad, Noshir A. Langrana, Ahmad Safari, Philip J. Whalen, Stephen C. Danforth, Structural quality of parts processed by fused deposition, Rapid Prototyp. J. 2 (1996) 4–19. doi:10.1108/13552549610732034.

[87] Comb, J.W., Priedeman, W.R. and Turley, P.W., FDM® Technology Process Improvements, in: Texas, 1994: pp. 42–9. http://sffsymposium.engr.utexas.edu/Manuscripts/1994/1994-06-Comb.pdf (accessed April 12, 2016).

[88] G.I.J. Salentijn, P.E. Oomen, M. Grajewski, E. Verpoorte, Fused Deposition Modeling 3D Printing for (Bio)analytical Device Fabrication: Procedures, Materials, and Applications,

Anal. Chem. 89 (2017) 7053–7061. doi:10.1021/acs.analchem.7b00828.

[89] O.S. Carneiro, A.F. Silva, R. Gomes, Fused deposition modeling with polypropylene, Mater. Des. 83 (2015) 768–776. doi:10.1016/j.matdes.2015.06.053.

[90] F. Ning, W. Cong, J. Qiu, J. Wei, S. Wang, Additive manufacturing of carbon fiber reinforced thermoplastic composites using fused deposition modeling, Compos. Part B Eng. 80 (2015) 369–378. doi:10.1016/j.compositesb.2015.06.013.

[91] H.L. Tekinalp, V. Kunc, G.M. Velez-Garcia, C.E. Duty, L.J. Love, A.K. Naskar, C.A. Blue, S. Ozcan, Highly oriented carbon fiber–polymer composites via additive manufacturing, Compos. Sci. Technol. 105 (2014) 144–150. doi:10.1016/j.compscitech.2014.10.009.

[92] P. Dudek, FDM 3D Printing Technology in Manufacturing Composite Elements, Arch. Metall. Mater. 58 (2013) 1415–1418. doi:10.2478/amm-2013-0186.

[93] K. Estelle, D. Blair, K. Evans, B.A. Gozen, Manufacturing of smart composites with hyperelastic property gradients and shape memory using fused deposition, J. Manuf. Process. 28 (2017) 500–507. doi:https://doi.org/10.1016/j.jmapro.2017.04.018.

[94] A.T. Miller, D.L. Safranski, K.E. Smith, R.E. Guldberg, K. Gall, Compressive cyclic ratcheting and fatigue of synthetic, soft biomedical polymers in solution, J. Mech. Behav. Biomed. Mater. 54 (2016) 268–282. doi:10.1016/j.jmbbm.2015.09.034.

[95] C.R. Rocha, A.R.T. Perez, D. a Roberson, Novel ABS-based binary and ternary polymer blends for material extrusion 3D printing, J. Mater. Res. 29 (2014) 1859–1866. doi:10.1557/jmr.2014.158.

[96] A.R. Torrado Perez, Defeating anisotropy in material extrusion 3D printing via materials development, 2015. http://search.proquest.com/docview/1709274119/abstract/F5CEEE3D9A2B47D3PQ/1 (accessed July 7, 2016).

[97] M.H. Bin Md Ansari, M.H. Irwan Bin Ibrahim, Thermal Characteristic Of Waste-Derived Hydroxyapatite (HA) Reinforced Ultra High Molecular Weight Polyethylene (UHMWPE) Composites For Fused Deposition Modeling (FDM) Process, IOP Conf. Ser. Mater. Sci. Eng. 165 (2017) 12014. doi:10.1088/1757-899X/165/1/012014.

[98] C.J. Schwartz, Investigation of the performance of articular cartilage and synthetic biomaterials in multi- directional sliding motion as in orthopedic implants by, Iowa State University, 2006. http://lib.dr.iastate.edu/rtd/3021.

[99] M.C. Sobieraj, C.M. Rimnac, Ultra high molecular weight polyethylene: mechanics, morphology, and clinical behavior, J. Mech. Behav. Biomed. Mater. 2 (2009) 433–443. http://www.sciencedirect.com/science/article/pii/S1751616108001197 (accessed October 24, 2016).

[100] P. Bracco, A. Bellare, A. Bistolfi, S. Affatato, Ultra-high molecular weight polyethylene: Influence of the chemical, physical and mechanical properties on thewear behavior. A review, Materials (Basel). 10 (2017). doi:10.3390/ma10070791.

[101] A. Mansson, Experiments - Moisture in 3D printing, (2016). https://www.antonmansson.com/moisture/ (accessed October 12, 2017).

[102] A. Ball, Polymer Processing, West. Carolina Univ. (n.d.). http://paws.wcu.edu/ballaaron/www/met366/modules/module5/mod5.htm (accessed May 1, 2017).

[103] A. V. Kuchuk, P. Borowicz, M. Wzorek, M. Borysiewicz, R. Ratajczak, K. Golaszewska, E. Kaminska, V. Kladko, A. Piotrowska, Ni-Based Ohmic Contacts to n -Type 4H-SiC: The Formation Mechanism and Thermal Stability, Adv. Condens. Matter Phys. 2016 (2016). doi:10.1155/2016/9273702.

[104] NinjaTek, NinjaFlex ® 3D Printing Filament: Flexible Polyurethane Material for FDM Printers, Manheim, PA, 2016.

[105] M. Hanifpour, C.F. Petersen, M.J. Alava, S. Zapperi, Mechanics of disordered auxetic metamaterials, arXiv Prepr. (2017) 1–6. http://arxiv.org/abs/1704.00943.

[106] D. Baykal, R.S. Siskey, R.J. Underwood, A. Briscoe, S.M. Kurtz, The Biotribology of PEEK-on-HXLPE Bearings Is Comparable to Traditional Bearings on a Multidirectional Pin-on-disk Tester, Clin. Orthop. Relat. Res. 474 (2016) 2384–2393. doi:10.1007/s11999-016-4989-7.

[107] ASTM, Standard Test Method for Wear Testing of Polymeric Materials Used in Total Joint, Am. Soc. Test. Mater. (2000) 1–16. doi:10.1520/F0732-00R11.2.

[108] E. Jones, S.C. Scholes, I.C. Burgess, H.E. Ash, A. Unsworth, Compliant layer bearings in artificial joints . Part 2 : simulator and fatigue testing to assess the durability of the interface between an elastomeric layer and a rigid substrate, 223 (2009) 1–12. doi:10.1243/09544119JEIM446.

[109] G.R. Higginson, Elastohydrodynamic Lubrication in Human Joints, Proc. Inst. Mech. Eng. 191 (1977) 217–223. doi:10.1243/PIME_PROC_1977_191_028_02.

[110] B.J. McEntire, R. Lakshminarayanan, D.A. Ray, I.C. Clarke, L. Puppulin, G. Pezzotti, Silicon Nitride Bearings for Total Joint Arthroplasty, Lubricants. 4 (2016) 35. doi:10.3390/lubricants4040035.

[111] K. Gardner, D. L.; O'Connor, P.; Oates, Low temperature electron microscopy of dog and guinea-pig hyaline articular cartilage, J. Anat. 132 (1981) 267–282. doi:10.1016/j.micron.2012.01.018.

[112] S.M. Kurtz, UHMWPE Biomaterials Handbook: Ultra High Molecular Weight Polyethylene in Total Joint Replacement and Medical Devices, William Andrew, 2015. https://books.google.com/books?id=j-sUBQAAQBAJ.

[113] M. Rogulska, A. Kultys, Aliphatic polycarbonate-based thermoplastic polyurethane elastomers containing diphenyl sulfide units, J. Therm. Anal. Calorim. 126 (2016) 225–243. doi:10.1007/s10973-016-5420-z.

[114] R.M. Trommer, M.M. Maru, W.L. Oliveira Filho, V.P.S. Nykanen, C.P. Gouvea, B.S. Archanjo, E.H. Martins Ferreira, R.F. Silva, C.A. Achete, Multi-Scale Evaluation of Wear in UHMWPE-Metal Hip Implants Tested in a hip Joint Simulator, Biotribology. 4 (2015) 1–11. doi:10.1016/j.biotri.2015.08.001.

[115] J.A. Williams, Wear and wear particles - Some fundamentals, Tribol. Int. 38 (2005) 863–870. doi:10.1016/j.triboint.2005.03.007.

[116] G.W.S. A.W.Batchelor, 14 Fatigue Wear, Tribol. Ser. 24 (1993) 657–681. doi:10.1016/S0167-8922(08)70588-1.

[117] T.R. Green, J. Fisher, M. Stone, B.M. Wroblewski, E. Ingham, Polyethylene particles of a "critical size" are necessary for the induction of cytokines by macrophages in vitro, Biomaterials. 19 (1998) 2297–2302. doi:10.1016/S0142-9612(98)00140-9.

[118] M.J. Nine, D. Choudhury, A.C. Hee, R. Mootanah, N.A.A. Osman, Wear debris characterization and corresponding biological response: Artificial hip and knee joints, Materials (Basel). 7 (2014) 980–1016. doi:10.3390/ma7020980.

[119] A. Bižal, J. Klemenc, M. Fajdiga, Evaluating the statistical significance of a fatigue-life reduction due to macro-porosity, Stroj. Vestnik/Journal Mech. Eng. 60 (2014) 407–416. doi:10.5545/sv-jme.2013.1453.

[120] A.T. Miller, D.L. Safranski, K.E. Smith, D.G. Sycks, R.E. Guldberg, K. Gall, Fatigue of injection molded and 3D printed polycarbonate urethane in solution, Polymer (Guildf). 108 (2017) 121–134. doi:10.1016/j.polymer.2016.11.055.

[121] J.J. Elsner, S. Portnoy, G. Zur, F. Guilak, A. Shterling, E. Linder-Ganz, Design of a Free-Floating Polycarbonate-Urethane Meniscal Implant Using Finite Element Modeling and Experimental Validation, J. Biomech. Eng. 132 (2010) 95001-95001–8. doi:10.1115/1.4001892.

[122] M. Shemesh, R. Asher, E. Zylberberg, F. Guilak, E. Linder-Ganz, J.J. Elsner, Viscoelastic properties of a synthetic meniscus implant, J. Mech. Behav. Biomed. Mater. 29 (2014) 42–55. doi:10.1016/j.jmbbm.2013.08.021.

APPENDIX - LIST OF CONFERENCE PRESENTATIONS

Center for Advanced Surface Engineering (CASE) Annual Meeting (Arkansas NSF EPSCoR). Student poster – Little Rock, AR, May 2016;

76th Annual Physical Electronics Conference (American Vacuum Society, AVS PEC). Student poster – Fayetteville, AR, June 2016;

72nd STLE Annual Meeting & Exhibition. Student poster – Atlanta, GA, May 2017;

Arkansas Biosciences Institute Fall Research Symposium. Student poster – Fayetteville, AR, October 2017;

Center for Advanced Surface Engineering (CASE) Annual Meeting (Arkansas NSF EPSCoR). Student Poster – Little Rock, AR, June 2017.